

1 **Distinct and additive effects of calorie restriction and rapamycin in aging skeletal**  
2 **muscle**

3  
4 Daniel J. Ham <sup>\*†1</sup>, Anastasiya Börsch <sup>\*†1</sup>, Kathrin Chojnowska<sup>1</sup>, Shuo Lin<sup>1</sup>, Aurel B.  
5 Leuchtmann<sup>1</sup>, Alexander S. Ham<sup>1</sup>, Marco Thürkauf<sup>1</sup>, Julien Delezie<sup>1</sup>, Regula Furrer<sup>1</sup>,  
6 Dominik Burri<sup>1</sup>, Michael Sinnreich<sup>2</sup>, Christoph Handschin<sup>1</sup>, Lionel A. Tintignac<sup>2</sup>, Mihaela  
7 Zavolan<sup>†1</sup>, Nitish Mittal<sup>\*†1</sup>, Markus A. Rüegg <sup>\*†1</sup>.  
8

9 †These authors contributed equally to the manuscript.

10 ‡ These authors contributed equally to the manuscript.

11 \*Corresponding authors email: [markus-a.ruegg@unibas.ch](mailto:markus-a.ruegg@unibas.ch); [nitish.mittal@unibas.ch](mailto:nitish.mittal@unibas.ch);  
12 [dan.ham@unibas.ch](mailto:dan.ham@unibas.ch).

13

14 **AFFILIATIONS**

15 1 Biozentrum, University of Basel, Basel, Switzerland

16 2 Department of Biomedicine, Pharmazentrum, University of Basel, Basel, Switzerland

17

18 **Abstract**

19 As global life expectancy continues to climb, maintaining skeletal muscle function is increasingly  
20 essential to ensure a good life quality for aging populations. Calorie restriction (CR) is the most potent  
21 and reproducible intervention to extend health and lifespan, but is largely unachievable in humans.  
22 Therefore, identification of “CR mimetics” has received much attention. CR targets nutrient-sensing  
23 pathways centering on mTORC1. The mTORC1 inhibitor, rapamycin, has been proposed as a potential  
24 CR mimetic and is proven to counteract age-related muscle loss. Therefore, we tested whether  
25 rapamycin acts via similar mechanisms as CR to slow muscle aging. Contrary to our expectation, long-  
26 term CR and rapamycin-treated geriatric mice display distinct skeletal muscle gene expression profiles  
27 despite both conferring benefits to aging skeletal muscle. Furthermore, CR improved muscle integrity  
28 in a mouse with nutrient-insensitive sustained muscle mTORC1 activity and rapamycin provided  
29 additive benefits to CR in aging mouse muscles. Therefore, RM and CR exert distinct, compounding  
30 effects in aging skeletal muscle, opening the possibility of parallel interventions to counteract muscle  
31 aging.

## 32 **Introduction**

33 Dietary or calorie restriction (CR) is the most potent and reproducible intervention to  
34 extend lifespan. However, CR as a human lifestyle is considered largely unachievable based on  
35 the sheer willpower required to maintain a low-calorie diet along with potential side effects  
36 including extreme leanness and cold sensitivity (1). In order to eventually translate the health  
37 benefits of CR into medical treatments for aging humans, a mechanistic understanding of how  
38 CR confers longevity is essential (2). CR, along with many of the interventions known to  
39 prolong lifespan, dampen the activity of nutrient-sensing pathways, which center around the  
40 mammalian target of rapamycin complex 1 (mTORC1), thereby alleviating protein synthetic  
41 burden and promoting intrinsic quality control processes, like autophagy (3). Findings that the  
42 mTORC1 inhibitor, rapamycin (RM), extends lifespan in yeast (4), flies (5), worms (6) and  
43 mice (7) strengthened the hypothesis that mTORC1 inhibition is fundamental to CR-induced  
44 lifespan extension (8).

45 Over the last century, global life expectancy has nearly doubled, but, as the World Health  
46 Organization recognized while declaring 2021-2030 the decade of healthy aging: “adding more  
47 years to life can be a mixed blessing if it is not accompanied by adding more life to years” (9).  
48 A well-functioning neuromuscular system is fundamental to ensure more life comes with more  
49 years. Since anabolic pathways, especially those involving mTORC1, promote both muscle  
50 growth (10, 11) and sarcopenia, the age-related loss of muscle mass (12), skeletal muscle is  
51 considered a potential sticking point for achieving both life extension and life quality via CR  
52 and RM. However, we have recently demonstrated that long-term RM treatment is  
53 overwhelmingly, although not entirely, beneficial for aging mouse skeletal muscle (13). While  
54 a thorough examination of whether long-term CR, spanning the time of sarcopenic development  
55 (20-28 months in mice (14)) counteracts phenotypic and molecular signatures of sarcopenia is  
56 still lacking, life-long CR appears to afford similar benefits as RM to aging skeletal muscle,

57 including a more stable neuromuscular junction (15) and slower age-related muscle loss (16,  
58 17). Could RM, therefore, function as a CR mimetic to slow muscle aging?

59 Studies in mice highlight that although both CR and RM blunt mTORC1 activity and  
60 promote autophagy (18, 19), their effects on insulin signaling strongly diverge, with CR  
61 improving and RM impairing glucose tolerance (19, 20). Similarly, molecular profiling studies  
62 in mouse liver have shown that the vast majority of acute transcriptomic, metabolomic (21) and  
63 proteomic responses to CR and RM are distinct (22). But is this a case of ‘all roads lead to  
64 Rome’, where CR and RM travel different paths to mTORC1 suppression, or do these two  
65 quintessential life-prolonging interventions travel different roads with distinct destinations? If  
66 the former is true, we reasoned that 1) the molecular and phenotypic signatures of long-term  
67 CR and RM in skeletal muscle should overlap; 2) the beneficial effects of CR should be lost if  
68 skeletal muscle mTORC1 activity remains high and; 3) the effects of RM should be lost in  
69 calorie-restricted mice.

70 Using repeated measurements of whole-body muscle function and body composition,  
71 multi-muscle gene expression profiling and extensive endpoint examination of isolated muscle  
72 function and fiber type properties, we first thoroughly characterized the impact of long-term  
73 CR starting from 15 or 20 months until 30 months of age, thus covering the period when  
74 sarcopenia develops. Compared to a weight-controlled, *ad libitum*-fed control group, CR mice  
75 improved whole-body and isolated relative muscle function and experienced a fast-to-slow shift  
76 in muscle fiber phenotype. While much of this phenotype was shared by RM treated mice (13),  
77 gene expression signatures of CR and RM were strikingly divergent, the only exception relating  
78 to the suppression of age-related increases in immune and inflammatory responses. In further  
79 opposition to overlapping functions, CR improved markers of muscle quality, including  
80 autophagy blockade as seen by P62 build up, plasma creatine kinase (CK) levels, centro-  
81 nucleated fibers and *in vitro* muscle function in a nutrient-insensitive, mTORC1-driven model  
82 of premature muscle aging, without suppressing mTORC1 activity. Most conclusively, long-

83 term RM treatment effectively counteracted skeletal muscle aging in both *ad libitum* and CR  
84 mice. We therefore demonstrate that RM and CR exert distinct and frequently additive effects  
85 on aging skeletal muscle, thereby opening the possibility of parallel interventions to counteract  
86 aging.

87

## 88 **RESULTS**

### 89 **Adaptations to calorie restriction favor whole-body muscle function but do not prevent** 90 **an age-related decline**

91 After habituation to single housing and the AIN-93M diet, 15- (CR<sub>15m</sub>) or 20- (CR<sub>20m</sub>)  
92 month-old mice underwent a weekly, stepwise reduction in food intake from 100% (3.2g) to  
93 90% (2.9g), 80% (2.6g), 70% (2.3g) and finally 65% (2.1g) of *ad libitum* levels until 30 months  
94 of age (Fig. 1A). After the initial month, calorie restricted mice continued to rapidly lose body  
95 mass for 2-3 months and then maintained a body mass between 21 and 26% below control mice  
96 from ~19 or 23 months to 30 months for CR<sub>15m</sub> and CR<sub>20m</sub> groups, respectively (Fig. 1B). Food  
97 intake normalized to body surface area indicated that calorie restricted mice do not fully  
98 compensate for reduced food intake through body mass reductions, partially adapting to the  
99 low-energy environment through energy sparing processes (Fig. 1C). After initially drawing on  
100 energy reserves, particularly fat (23), calorie restricted mice display a range of adaptations to  
101 cope with the shortfall in energy intake, including improving energy absorption, reducing non-  
102 essential organ mass and lowering body temperature and energy expenditure (24). Compared  
103 to controls, 24-month-old calorie restricted mice had larger proportional differences in fat mass  
104 than lean mass, but smaller absolute differences (Fig. 1D). A progressive, age-related loss of  
105 whole-body fat mass in control mice narrowed the difference in fat, but not lean mass between  
106 CR and CON mice at 30 months of age.

107 Repeated all-limb grip strength measures spanning the treatment period show that the  
108 progressive age-related loss of absolute grip strength was similar in both control and calorie

109 restricted mice ( $P < 0.001$ ; Fig. 1E, upper). However, due to the initial rapid loss of body mass,  
110 calorie restricted mice strongly increased relative grip strength ( $\text{N} \cdot \text{g body mass}^{-1}$ ) over the  
111 initial 2-3 months before displaying a similar age-related decline in relative grip strength as  
112 control mice from 22 to 30 months (Fig. 1E, lower). As such, compared to the initial recording  
113 (15 or 20 months), relative grip strength significantly declined across the treatment period in  
114 control mice ( $P < 0.001$ ), but not in CR mice. However, when compared to the 22-month  
115 recording, the decline in relative grip strength was not different between control ( $P < 0.002$ ) and  
116 calorie restricted ( $P < 0.001$ ) mice at 30 months. Consistent with improved relative strength,  
117 calorie restriction potently improved inverted grid-hang time compared to both 10mCON and  
118 30mCON groups (Fig. 1F;  $P < 0.001$ ). Similarly, voluntary running activity over a 24 h period  
119 was consistently improved in calorie restricted mice across the trial (Fig. 1G;  $P < 0.01$ ).

120         After an overnight fast for all groups, calorie restricted mice showed a marked increase  
121 in glucose tolerance and significantly lower blood glucose levels than 8 and 24-month-old  
122 control mice at each point after glucose injection (Fig. 1H). CR also lowered peak glucose (Fig.  
123 1I) and the area under the curve (AUC; Fig. 1J). Despite similar body mass and whole-body fat  
124 mass, 24-month-old control mice showed lower blood glucose at 30 and 60 min after glucose  
125 injection as well as a lower peak glucose and AUC than 8-month-old control mice. Similarly,  
126 improvements in glucose tolerance have been observed between 20 and 28 months of age in  
127 wild type mice (25) and also in mice genetically modified to have high muscle fiber mTORC1  
128 activity (26), a commonly observed feature of sarcopenic muscle (13, 27-29).

129         While daylight regulated whole-body metabolism in control mice; with energy  
130 expenditure, activity and RER all high at night and low during the day; metabolism in CR mice  
131 centered around food availability (Fig. 1K and Fig. S1A-F). In CR mice, energy expenditure  
132 (Fig. 1K upper) and activity (Fig. 1K middle) were tightly restricted to the hours immediately  
133 before and immediately after their 5 pm food allocation. Despite displaying characteristic  
134 anticipatory increases in activity and energy expenditure prior to food, RER remained at around

135 0.7 (Fig. 1K lower), indicating almost exclusive fat utilization, before a food- and therefore  
136 glucose availability-related increase during night-time hours. In line with lower food intake per  
137 body surface area in CR mice (Fig. 1C), mean energy expenditure per body surface area was -  
138 8.8 and -8.5% lower ( $P<0.05$ ) during day-time hours and -16.6% and -21.0% lower during  
139 night-time hours at 25 and 30 months of age in CR than control mice (Fig. S1C). Together,  
140 these data indicate that calorie restricted mice shed excess tissue mass and induce metabolic  
141 adaptations to minimize energy use and maximize energy uptake when scarce food becomes  
142 available. Since the extent of metabolic adaptations and lifespan extension increase in parallel  
143 with that of calorie restriction, these adaptations are thought to be central to the health and  
144 longevity benefits of CR (24, 30). While these changes initially lead to a substantial increase in  
145 relative grip strength, calorie restricted mice also display a progressive age-related loss of grip  
146 strength indicating that while CR clearly improves muscle functional parameters, mice are not  
147 entirely spared from muscle aging.

148

#### 149 **Calorie restriction promotes a fast-to-slow muscle phenotype transition**

150 Aging reduced absolute (Fig. S1G) and relative (mg/g body mass) mass (Fig. 2A) in all  
151 measured muscles. CR further reduced absolute muscle mass in the fast-twitch quadriceps  
152 (QUAD), gastrocnemius (GAS), tibialis anterior (TA), plantaris (PLA), extensor digitorum  
153 longus (EDL) and triceps brachii (TRI) muscles but not in the slow-twitch SOL muscle (Fig.  
154 S1G). When accounting for body mass, muscle mass was similar in 30mCON and 30mCR  
155 groups for all fast-twitch muscles, except quadriceps, which along with the slow-twitch soleus  
156 muscle were significantly heavier relative to body mass in 30mCR than 30mCON mice (Fig.  
157 2A). While correlation graphs indicate that the muscle-to-body mass ratio was similar for all  
158 fast twitch muscles, SOL mass was clearly higher for a similar body mass in 30mCR than  
159 30mCON mice (Fig. 2B). In line with measures of body composition, CR reduced the absolute  
160 mass of all major organs (heart, spleen, kidney, liver) as well as epididymal white and

161 interscapular brown fat depositions and prevented the age-related accumulation of non-  
162 functional mass (i.e. seminal vesicles; Fig. S1H). Proportional to body mass, CR preserved  
163 heart, liver and brown fat mass while shedding white fat, kidney and spleen mass (Fig. S1I).

164 Preferential sparing of slow-twitch muscle was also observed in measures of isolated  
165 muscle function in the fast EDL and slow SOL muscle (Fig. 2C-F). Long-term CR did not alter  
166 the strong age-related reduction in absolute tetanic force in the SOL but further lowered tetanic  
167 force in EDL muscle from 100-250 Hz (Fig. 2C, left). In response to repeated stimulations,  
168 tetanic force dropped more rapidly in the 10mCON group than either 30mCON or 30mCR  
169 groups (Fig. 2C, right). Despite producing significantly greater absolute force at the start of the  
170 assay in both SOL and EDL, force in the 10mCON was not different to the other groups after  
171 45 contractions in SOL and significantly lower than both other groups after 20 contractions in  
172 the EDL (Fig. 2C, right). After 45 contractions, 30mCR mice produced significantly more force  
173 than 30mCON mice in SOL muscle, but less in EDL muscle. In line with body mass-normalized  
174 grip-strength measurements, calorie restriction completely prevented the age-related loss of  
175 SOL and EDL peak tetanic force (Fig. 2D). This was at least partially the result of improved  
176 muscle quality in 30mCR mice, which showed significantly higher specific muscle force,  
177 representing peak force normalized to muscle cross-sectional area, in both SOL and EDL  
178 muscle (Fig. 2E). Aging slowed muscle twitch properties with significantly longer time-to-peak  
179 tension in SOL and a longer half-relaxation time in the EDL muscle (Fig. 2F). CR augmented  
180 this phenotype, with 30mCR mice showing significantly longer time-to-peak tension and half-  
181 relaxation time than either 10mCON or 30mCON in both SOL and EDL muscles (Fig. 2F).

182 Consistent with the CR-induced fast-to-slow shift in muscle function properties,  
183 preferential protection of slow-twitch muscle mass, and improvements in whole-body  
184 endurance, fiber type-specific analysis of muscle cross sections showed a strong increase in the  
185 proportion of total cross-sectional area made up by slower fiber types in soleus (SOL), extensor  
186 digitorum longus (EDL), tibialis anterior (TA) and triceps brachii (TRI; Fig. 1G-H). Although



187 a fast-to-slow transition was seen in all muscles analyzed, each muscle displayed specific  
188 changes in fiber type size and number (Fig. S2A-E). Compared to 10mCON and 30mCON, the  
189 proportional area of type I fibers in SOL, IIX fibers in EDL, IIA fibers in TA and both IIA and  
190 IIX fibers in TRI was higher while the proportional area of IIX in SOL and IIB in EDL, TA and  
191 TRI was lower for 30mCR (Fig. 1G-H). The largest and fastest type IIB fibers appeared to be  
192 the most expendable for calorie restricted mice, with significant reductions in both proportional  
193 fiber number (Fig. S2B) and minimum fiber feret (Fig. S2C-D) in EDL, TA and TRI muscles.  
194 On the other hand, the size of slower IIA fibers and of intermediate IIX fibers were less affected  
195 by both age and CR (Fig. S2C-D) and CR increased their proportional number (Fig. S2B). Since  
196 slower-type fibers are more resistant to age-related atrophy, the CR-induced fast-to-slow fiber-  
197 type transition, despite the absolute decrease in muscle mass, may ultimately preserve muscle  
198 function in aging mice as seen with other interventions (31).

199

## 200 **Calorie restriction and rapamycin induce distinct transcriptomic changes**

201 While the overt aging phenotype in calorie-restricted mice is distinct from that observed  
202 in mice treated with rapamycin over the same period (13), calorie restriction is thought to  
203 counteract aging in large part by suppressing nutrient-induced activation of mTORC1 activity  
204 (32). If this were the case, then long-term CR and RM should induce a common core gene  
205 expression signature in aging muscle. To address this hypothesis, we performed mRNA-  
206 sequencing on four muscles (GAS, TA, TRI and SOL) from six 30-month-old calorie restricted  
207 mice and compared the profiles with our previously reported 10mCON, 30mCON and 30mRM  
208 data sets (Fig. 3A) (13).

209 To determine the overlap in core gene expression signatures induced by age, CR and RM,  
210 we first defined the specific effect of each condition separately by performing principal  
211 component (PC) analysis on data from all four muscles for each of the following four  
212 comparisons: 10mCON vs. 30mCON (PC<sub>10m-30m</sub>); 30m vs. 30mCR (PC<sub>30m-CR</sub>); 30m vs.

213 30mRM ( $PC_{30m-RM}$ ;) and; 30mCR vs. 30mRM ( $PC_{CR-RM}$ ;) . Aside from three prominent PC  
214 patterns representing the inter-muscle gene expression differences we have previously reported  
215 (13), we found that for each comparison there was one PC (PC3 or PC4) that showed a clear  
216 between-group expression pattern difference common to all four muscles (Fig. 3B). To check  
217 to what extent genes aligned with  $PC_{30m-30m}$  (aging effect),  $PC_{30m-CR}$  (CR effect) and  $PC_{30m-}$   
218  $RM$  (RM effect) overlapped, we created Venn diagrams for aging and CR, aging and RM and  
219 CR and RM effect comparisons, respectively (Fig. 3C). Strikingly, RM reversed and CR  
220 accentuated the vast majority of commonly regulated, age-related gene expression changes.  
221 Likewise, genes that responded to both CR and RM treatments were predominately regulated  
222 in the opposite direction. Gene ontology analysis showed that genes involved in extracellular  
223 matrix remodeling were highly represented in overlapping genes from each of the three  
224 comparisons (Fig. 3D).

225       Next we visualized the log-fold changes in expression for each gene aligned to any of the  
226 PCs displayed in Fig. 3B. Hierarchical clustering based on the Euclidean distance of these  
227 changes rendered 8 gene clusters with distinct gene expression patterns (Fig. 3E). While CR  
228 and RM both tended to suppress a group of genes related to the innate immune response which  
229 are upregulated with age in cluster 2, CR and RM displayed strikingly opposing gene expression  
230 patterns throughout most other clusters as well as distinct CR (cluster 3) and RM (cluster 4)  
231 effects related to lipid metabolism and insulin signaling, respectively. While RM reversed, or  
232 partially reversed, age-related gene expression changes in many clusters, CR augmented age-  
233 related signaling such that gene expression differences between CR and RM were exaggerated.  
234 This pattern was particularly prevalent in cluster 5 and 8. Cluster 5 represents genes increased  
235 with age, further increased by CR and suppressed by RM, while cluster 8 displays the opposite  
236 pattern. The top DAVID gene ontology terms associated with cluster 5 relate to changes in  
237 metabolism while those associated with cluster 8 relate to the extracellular matrix (Fig. S3).  
238 The common effects of CR and RM observed in cluster 2 primarily relate to immune responses.

239 In line with these findings, circulating levels of the pro-inflammatory cytokines tended to be  
240 lower in both calorie-restricted and rapamycin-treated mice, with the exception of IFN- $\gamma$  which  
241 tended to be suppressed by RM, but not CR (Fig. 1F).

242 These striking differences in gene expression patterns led us to wonder whether the  
243 signaling responses to CR and RM represent distinct paths to a common destination centered  
244 around immune and inflammatory suppression, i.e. an ‘all roads lead to Rome’ scenario, or  
245 whether CR and RM act on distinct muscle aging processes. If the latter is true, we reasoned  
246 that calorie restriction should benefit aging skeletal muscle independent of skeletal muscle  
247 mTORC1 suppression.

248

#### 249 **Calorie restriction attenuates muscle mTORC1-driven premature sarcopenia without** 250 **suppressing mTORC1**

251 To address this hypothesis, we calorie restricted muscle-specific TSC1-knockout  
252 (TSCmKO) mice, which display sustained, nutrient-insensitive mTORC1 activation (33) and  
253 an accelerated aging phenotype (13, 26). At 3 months of age, TSCmKO mice display high  
254 muscle mTORC1 activity and impaired autophagy, but mild phenotypic features. From ~6 to  
255 12 months of age, TSCmKO display a progressive sarcopenia-like phenotype including muscle  
256 atrophy and weakness as well as accumulation of P62-labelled proteins and aggregates (33),  
257 which are also, to some degree, features of sarcopenia (13, 34). We therefore tested whether 7  
258 months of calorie restriction starting at 3 months of age can ameliorate the muscle fiber  
259 mTORC1-driven sarcopenic phenotype in TSCmKO mice (Fig. 4A). CR induced similar  
260 changes in body (Fig. 4B), fat (Fig. 4C) and lean (Fig. 4D) mass in both TSCmKO and WT  
261 control mice and comparable with those observed in naturally aging mice (Fig. 1B, D). *Ad*  
262 *libitum*-fed TSCmKO mice (TSC-AL) were significantly lighter than their *ad libitum*-fed  
263 controls (WT-AL) at 9.5 months. This was primarily due to a divergence in fat depositions from  
264 4.5 months, with WT-AL gaining (+18%;  $P < 0.05$ ) and TSC-AL losing (-25%;  $P < 0.05$ ) fat mass

265 over the period (Fig. 4B). Body mass and composition were comparable in calorie restricted  
266 TSCmKO (TSC-CR) and WT (WT-CR) mice, aside from a tendency for lower fat mass in TSC-  
267 CR than WT-CR at 6.5 months (Fig. 4B). CR also induced the characteristic metabolic  
268 adaptations in patterns of energy expenditure (Fig. 4E) and RER (Fig. 4F) equally in both WT  
269 and TSCmKO mice and comparable with those observed in naturally aging mice (Fig. 1K).

270 To confirm that mTORC1 activity was not suppressed in TSC-CR mice, we investigated  
271 the phosphorylation status of mTOR (S2448) and its key downstream targets S6 (S240/244 and  
272 S235/237) and 4EBP1 (S65) as well as AKT (S473) and PRAS40 (T246), which are dampened  
273 by inhibitory feedback from the mTORC1 target S6K1 via IRS1 (35) in TA and/or GAS muscle  
274 using Western blot analysis (Fig. 4G-H and S4A-B & D). TSC-AL mice displayed the  
275 stereotypical markers of chronic mTORC1 activation, including high phosphorylated mTOR,  
276 S6 and 4EBP1 as well as lower phosphorylated AKT and PRAS40. Despite reducing the  
277 availability of mTORC1-activating nutrients (e.g. amino acids), CR was largely incapable of  
278 suppressing mTORC1 activity or alleviating feedback inhibition of AKT in TSC-CR mice (Fig.  
279 4G-H and S4A-B, E). Together, these results indicate that CR induces typical changes in whole-  
280 body composition and metabolism independent of muscle mTORC1 activity and without overt  
281 negative side-effects.

282 Despite a lack of effect on mTORC1 activity, CR robustly improved whole-body  
283 measures of muscular endurance (Hang test, Fig. 4I) and coordination (rotarod, Fig. 4J),  
284 independent of genotype. Likewise, CR improved or tended to improve both specific force (Fig.  
285 4K) and peak tetanic force normalized to body mass (Fig. 4L) in isolated SOL and EDL muscle  
286 in both WT and TSCmKO mice. As we observed in aging WT mice, CR induced a slowing of  
287 muscle twitch properties, particularly in the SOL muscle (Fig. 4M-N), although fatigability was  
288 not significantly affected (Fig. 4O).

289 As a result of chronic mTORC1 activity-induced phosphorylation of ULK1 and thereby  
290 autophagy blockade, old (9-12 months) TSCmKO mice display strong cytosolic and aggregated

291 P62 accumulation in muscle fibers and an associated increase in signs of muscle degeneration,  
292 including high levels of plasma CK and centro-nucleated, regenerating fibers (33). Indeed,  
293 TSC-AL mice displayed a strong increase in P62 aggregate- and cytosolic-positive fibers (Fig.  
294 5A-C), P62 protein accumulation in muscle lysates (Fig. 5D), plasma CK activity (Fig. 5E) and  
295 centro-nucleated fibers (Fig. 5F). Strikingly, CR almost completely alleviated P62  
296 accumulation and signs of muscle degeneration. Despite the strong reduction in P62 protein  
297 levels, CR did not suppress *Sqstm1* expression, which encodes for the P62 protein, nor the other  
298 autophagy induction mediators *Ctsl*, *Gabarapl2*, *Bnip3*, *Atg7* or *Map1lc3a* (Fig. 5C). Likewise,  
299 the mTORC1-mediated phosphorylation of ULK1 (S757), the LC3II/LC3I ratio and protein  
300 levels of beclin1 and BNIP3 were all unaltered by CR (Fig. 5I-K).

301 Endoplasmic reticulum (ER) stress and activation of the unfolded protein response (UPR)  
302 is also a hallmark of chronic muscle mTORC1 activation (26). CR did not reduce signs of ER  
303 stress in TSCmKO mice, including increased levels of ATF4, FGF21 and BiP (Fig. S4C-D).  
304 However, CR altered the response to ER stress, blunting the mTORC1-driven upregulation of  
305 *Trib3* (Fig. 5L), which can bind and inhibit the breakdown of P62, while inducing *Xbp1* (Fig.  
306 5M), encoding a UPR-inducing transcription factor (36). CR also induced the expression of  
307 *Keap1* (Fig. 5N), a gatekeeper protein for the NRF2-induced stress response that can be  
308 sequestered by P62, thereby preventing it from binding and preventing NRF2 nuclear  
309 translocation. While initially cytoprotective, chronic NRF2-induced activation of the stress  
310 response is deleterious (37). In line with a CR-induced suppression of NRF2 activity by *Keap1*  
311 upregulation, the mTORC1-induced upregulation of *Gsta1* expression, an NRF2 target, was  
312 strongly suppressed in TSC-CR mice (Fig. 5O).

313 Together, these data strongly support the idea that CR can improve muscle proteostasis,  
314 integrity and function without suppressing mTORC1 activity. But is the reciprocal also true, or  
315 are the beneficial effects of rapamycin-induced mTORC1 suppression on aging skeletal muscle  
316 already captured by CR? In other words, would rapamycin also slow muscle aging in CR mice?

317

318 ***CR and RM have distinct and often additive beneficial effects on aging skeletal muscle.***

319 To directly determine whether RM and CR exert non-overlapping effects in aging skeletal  
320 muscle, *ad libitum*-fed (CON) and 35% calorie restricted (CR) male C57BL/6 mice were fed a  
321 standardized AIN-93M diet containing either encapsulated rapamycin (RM and CR+RM) or an  
322 equivalent amount of encapsulating vehicle (Eudragit; CON and CR) starting from 19 months  
323 of age (Fig. 6A). Based on body mass and food intake data from our initial study and a target  
324 dose of  $\sim 4 \text{ mg}\cdot\text{kg}^{-1}\cdot\text{day}^{-1}$  rapamycin, 42 and 48  $\text{mg}\cdot\text{kg}^{-1}$  of active encapsulated rapamycin was  
325 incorporated into the diet of RM and CR+RM groups, respectively. Consistent with our  
326 previous results, body mass loss compared to pre-trial levels was observed from 25 months in  
327 CON mice and from 20 months in RM-treated mice. After the initial adjustment to reduced  
328 food intake by 20 months of age, CR and CR+RM mice also displayed an age-related decline  
329 in body mass from around 26 months (Fig. 6B). Food intake, normalized to body surface area,  
330 was relatively stable over the treatment period in CON and RM mice, while CR and CR+RM  
331 mice showed a steady increase in normalized food intake from 20 months of age following an  
332 initial steep decline (Fig. 6C). RM did not alter the CR or age-related decline in whole-body fat  
333 mass and despite reducing lean mass in *ad libitum* fed mice, RM did not alter the CR-induced  
334 decline in whole-body lean mass (Fig. 6D).

335 Repeated grip strength measurements spanning the treatment period showed a clear RM-  
336 induced attenuation in the progressive loss of both absolute and body mass normalized grip  
337 strength (Fig. 6E) starting at 24 months of age. CR also induced a strong increase in body mass  
338 normalized grip strength between 19 and 22 months, independent of RM treatment. RM and  
339 CR also induced distinct changes in voluntary wheel running activity. While CR increased both  
340 day and night-time running distance independent of RM treatment, RM increased night-time  
341 running distance independent of CR (Fig. 6F-G). CR also potently improved inverted grid-hang  
342 time independent of RM treatment (Fig. 6H).

343 RM and CR individually induced changes in whole-body metabolism consistent with our  
344 previous observations (13) (Fig. I-J). RM induced a consistent increase in energy expenditure  
345 normalized to body surface area in control mice, but not in CR mice (Fig. 6I), consistent with  
346 both RM and CR reducing non-functional tissue mass (Fig. S5B-C). In contrast, RM blunted  
347 both the CR-induced increase in RER during the first half of the night and the CR-induced  
348 decrease in RER during day-time hours (Fig. 6J). Since prolonged RM treatment is known to  
349 inhibit mTORC2 and thereby glucose uptake, we wondered whether alterations in blood  
350 glucose or feeding behavior may explain the effect of RM on whole-body fuel utilization. Blood  
351 glucose was not different between CON and RM or between CR and CR+RM groups at 8 am  
352 or at 6 pm after a 10 h fast (Fig. 6K). Likewise, RM did not alter the blood glucose response to  
353 the reintroduction of food between 6pm and 12pm (Fig. 6K). CR mice ate their 2.1 g food  
354 allocation at a higher rate than *ad libitum*-fed mice (Fig. 6L). Interestingly, CR+RM mice ate  
355 their food allocation more slowly than CR mice, which may serve as a strategy to prevent high  
356 blood glucose levels in the face of a RM-induced impairment in glucose uptake.

357 Next we used 2-WAY ANOVAs to determine whether CR and RM also exerted distinct,  
358 independent effects on muscle mass. Consistent with improvements in whole-body muscle  
359 function, significant CR main effects were observed for relative TA, QUAD, EDL, PLA, GAS,  
360 brachioradialis (BR) and biceps brachii (BIC) muscle mass (Fig. 7A). Again, the effects of RM  
361 were either distinct or additive to those of CR, with significant RM main effects for TA, QUAD,  
362 EDL, PLA, BR, BIC and TRI. As we have previously observed, specific muscles have different  
363 responses to specific interventions (13). RM increased both relative and absolute muscle mass  
364 in the TRI muscle, while CR did not affect relative mass and reduced absolute TRI muscle mass  
365 (Fig. 7A and S5A). On the other hand, CR, but not RM improved relative GAS muscle mass,  
366 while CR significantly reduced and RM tended to reduce absolute GAS mass. The only  
367 interaction effect for RM and CR was observed for the SOL muscle, where RM improved  
368 relative muscle mass in CR mice but not *ad libitum* fed mice.

369 In line with the beneficial effects of RM treatment on whole-body muscle function and  
370 muscle size, independent of *ad libitum* or restricted feeding, RM main effects for *in vitro* muscle  
371 function properties were observed in the slow-twitch soleus muscle and to a lesser extent the  
372 fast-twitch EDL muscle (Fig. 7B-F). CR resulted in significant reductions in absolute tetanic  
373 force at multiple stimulation frequencies in the SOL (Fig. 7B, upper) and EDL (Fig. 7B, lower).  
374 RM significantly increased absolute tetanic force from a stimulation frequency of 20Hz in SOL,  
375 but not EDL muscle. Despite initial contraction forces below that of *ad libitum* fed mice, tetanic  
376 force in calorie restricted mice approached that of *ad libitum*-fed mice after 20 contractions in  
377 SOL (Fig. 7C, upper) and from 30-35 contractions in EDL (Fig. 7C, lower). RM, but not CR,  
378 induced significant increases in peak tetanic force normalized to body mass in both SOL (Fig.  
379 7D, upper) and EDL (Fig. 7D, lower). Rapamycin also induced a significant increase in muscle  
380 quality, as evidenced by higher specific forces in SOL muscle (Fig. 7E, upper) independent of  
381 feeding status and in EDL muscle (Fig. 7E, lower) from *ad libitum* fed mice. Analysis of muscle  
382 twitch properties show that RM slows SOL time-to-peak tension (TPT), while CR slowed EDL  
383 TPT (Fig. 7F). RM, CR and CR+RM mice all had longer half-relaxation times in SOL muscle,  
384 while CR induced a slowing of half-relaxation time in EDL.

385 Finally, we have shown that CR promotes a fast-to-slow fiber type transition (Fig. 2G-H)  
386 while RM also promotes a fast-to-slow fiber type transition and additionally increases the size  
387 of IIA and IIX fibers (13). Based on the preferential effect of both CR and RM on slow-twitch  
388 fibers and our previous observations that RM exerts negative side effects in some hindlimb  
389 muscles that may relate to their susceptibility to denervation, we analyzed the fiber-type  
390 composition and fiber cross sectional area in BR muscle, a forelimb muscle involved in  
391 grasping and arm flexion that contains a high proportion of IIA and IIX fibers (Fig. 7G-J). In  
392 BR muscle, both CR and RM independently increased the size of IIA and IIX fibers, with main  
393 effects for both treatments (Fig. 7H). Likewise, both CR and RM showed main effects for higher  
394 IIA fiber number and lower IIB fiber number (Fig. 7I), an effect also induced by age alone.



395 Together, the increase in IIA fiber size and number and the parallel decrease in IIB fiber number  
396 observed with age, CR and RM resulted in a change in proportional total fiber area from 13.6,  
397 37.3 and 49.1% for IIA, IIX and IIB fibers in 10-month-old adult mice to 38.1, 46.6 and 15.3%  
398 for IIA, IIX and IIB fibers in CR+RM treated mice (Fig. 7J).

399 Together, these data confirm that both CR and RM treatment exert distinct and often  
400 additive effects on whole-body muscle function and metabolism, the size and fiber type  
401 composition of specific muscles as well as isolated muscle function properties. Therefore, these  
402 findings support the idea that long-term mTORC1 suppression via RM can benefit aging  
403 skeletal muscle independent of CR.

404

## 405 **DISCUSSION**

406 The mechanism underlying the potent and robust anti-aging effects of CR have long  
407 fascinated the research community. An early theory proposed mTORC1 suppression as a central  
408 part of CR-induced longevity (8). Research showing long-term RM treatment extended lifespan  
409 in mice seemed to confirm this theory (7). However, despite both CR and RM blunting  
410 mTORC1 activity and promoting autophagy (18, 19), their effects on insulin signaling and  
411 glucose tolerance diverge (19, 20) and molecular profiles following short-term CR and RM in  
412 adult mouse liver show predominately distinct signatures (21, 22). Our multi-muscle  
413 transcriptomic data from 30-month-old mouse muscle support the concept that CR and RM  
414 have distinct mechanisms. Importantly, our study compares the effects of CR and RM treatment  
415 during the entire period of sarcopenic development (15 to 30 months), therefore representing  
416 both signaling responses to CR and RM as well as the cumulative effect of the treatments on  
417 age-related signaling. To improve the current understanding of the molecular mechanisms  
418 contributing to sarcopenia, we made our data publicly available through the user-friendly web  
419 application SarcoAtlas (<https://sarcoatlas.scicore.unibas.ch/>), building on our previously  
420 released sarcopenia data sets (13, 14).

421 The divergent gene expression patterns induced by CR and RM do not necessitate that  
422 entirely non-overlapping mechanisms are responsible for the beneficial effects of CR and RM.  
423 Rather, while starting from different points, these treatments could converge on the same  
424 effector pathways. Here we addressed the question of whether CR-induced mTORC1  
425 suppression is sufficient to make RM redundant and vice versa, and provided definitive  
426 evidence that CR and RM exert non-overlapping and often complementary effects in aging  
427 mouse skeletal muscle. Specifically, CR improves skeletal muscle function and quality  
428 independent of mTORC1 suppression and RM improves skeletal muscle function in CR mice.  
429 While mTORC1 inhibition as a strategy to fight aging arose from attempts to pharmacologically  
430 reproduce CR, the implications stemming from the apparent invalidation of this assumption are  
431 far greater to the aging field. Assuming that a true CR mimetic can eventually be identified, the  
432 prospect of multiple, additive interventions to slow aging is an exciting prospect.

433 While the specific mechanisms responsible for the pro-longevity effects of CR have  
434 proved challenging to pin down, many plausible theories have been developed. The  
435 evolutionary model of CR proposes that under energy scarcity, an organism actively allocates  
436 energy towards somatic maintenance at the expense of reproduction, thereby extending lifespan  
437 in the hope that circumstances will sufficiently improve to once again support reproduction (38,  
438 39). This theory is supported by observations that CR promotes the expression of maintenance  
439 and repair processes (40, 41). Signs of a CR-induced promotion of somatic maintenance was  
440 also observed in TSCmKO mice in the absence of mTORC1 suppression or reduced ER stress  
441 (Fig. 5). A CR-mediated induction of the somatic maintenance genes *Xbp1* and *Keap1* was  
442 associated with less P62 accumulation and improved skeletal muscle integrity (Fig. 5),  
443 highlighting the fact that skeletal muscle fiber mTORC1 suppression is not solely responsible  
444 for the beneficial effects of CR on muscle homeostasis.

445 The evolutionary model assumes that CR-induced physiological changes are inherently  
446 pro-longevity, however, when returned to an energy-rich diet, calorie restricted *Drosophila*

447 *melanogaster* reproduce less and experience greater mortality than their age-matched, non-  
448 restricted counterparts (2). Likewise, the beneficial effects of CR are quickly lost upon  
449 refeeding in rodents (42) and in humans, metabolic adaptations to CR promote strong weight gain  
450 upon refeeding (43). Therefore, rather than actively promoting longevity, CR may provide an  
451 escape from the cost of an energy-rich diet (2). The fact that sedentary, *ad libitum*-fed mice  
452 often become obese in aging studies<sup>12</sup> and that the propensity of mouse strains to become obese  
453 strongly correlates with the longevity effects of CR (44) support this theory. Importantly, in our  
454 study we used a combination of an AIN-93 maintenance diet and a controlled feeding regime  
455 to limit the food intake of *ad libitum*-fed mice with a penchant for overeating (Fig. 1), thereby  
456 limiting the potential negative effects of an obese and unhealthy control group, a common  
457 criticism of CR experiments (44).

458         An alternate theory proposes that rather than an evolved, programmed tradeoff between  
459 somatic maintenance and reproduction, the pro-longevity effects of CR may simply result from  
460 a passive, serendipitous response to metabolic stress (2) such as a lower metabolic rate (45),  
461 reduced mTORC1 activity (8) or hormetic response (46). In line with such an interpretation,  
462 long-term CR did not slow the absolute loss of all-limb grip strength nor did it reverse age-  
463 related gene expression changes. However, the CR-induced alterations in body composition led  
464 to marked improvements in body mass-normalized grip strength, which proceeded to decline  
465 with age in line with *ad libitum*-fed mice, but from a new higher starting point (Fig. 1 and 6).  
466 Irrespective of the permanence of CR-induced longevity and whether the effects are actively or  
467 passively conferred, the strong link between CR and beneficial health and lifespan outcomes  
468 means that closely examining the molecular and physiological responses to CR is a promising  
469 avenue to identify pathways and phenotypes that can be exploited to improve muscle function  
470 and consequently, the quality of life of aging individuals. The same is true for the pro-longevity  
471 and anti-sarcopenic effects of rapamycin. While our rationale for comparing these two  
472 interventions originally centered on identifying a core set of pathways regulated by aging and

473 commonly counter-regulated by CR and RM, our data show that CR and RM induce strikingly  
474 distinct gene expression profiles, with those genes and pathways that do overlap being regulated  
475 in predominately opposing directions (Fig. 3).

476 For example, CR specifically increases genes involved in lipid metabolism and RM  
477 specifically suppresses genes involved in insulin signaling, while the strongest counter-  
478 regulated gene expression cluster maps to ECM remodeling, including many collagen genes,  
479 which are reduced in aging muscle, restored by rapamycin but further decreased by CR. ECM  
480 gene expression coincides with changes in muscle size, increases during muscle hypertrophy  
481 (47), and decreases during experimental muscle atrophy (48) as well as sarcopenia in rodents  
482 (13, 14, 49, 50). Declining collagen expression has also been linked to organismal aging, while  
483 autophagy-inducing interventions restore collagen expression and promote longevity (51, 52).  
484 While this opposing action of CR and RM on ECM gene expression could be seen as  
485 counteractive, it may also represent different means of addressing the same perturbation. That  
486 is, age-related stressors can be counteracted by either blunting the perturbation or enhancing  
487 the inherent coping mechanisms. Indeed, gene expression profiling studies show that changes  
488 in gene expression resulting from mutations in mice that shorten lifespan positively correlate  
489 with mutations and interventions that extend lifespan (53). In other words, organisms naturally  
490 boost stress responses to cope with life-shortening perturbations, while interventions that  
491 moderately stimulate these stress responses, such as CR, extend lifespan. Alternatively, changes  
492 in ECM gene expression may simply reflect changes in protein turnover or absolute muscle size  
493 induced by the treatment. In line with this hypothesis, CR blunts and RM boosts polysome  
494 loading, an indicator of protein turnover, in skeletal muscle (22). The complexity of biological  
495 responses to aging and treatments such as CR and RM make interpreting directionality of gene  
496 expression changes inherently challenging. It is therefore imperative that molecular profiles be  
497 accompanied by thorough phenotypic characterizations.

498 Perhaps the most strikingly consistent muscle phenotype displayed by CR mice was a  
499 fatigue resistant, fast-to-slow muscle fiber property switch, including an increase in number and  
500 proportional cross sectional area covered by slower-type fibers across five different muscles as  
501 well as slower twitch properties (Fig. 2 and 7) and higher whole-body relative muscle endurance  
502 (Fig. 1 & 6). A similar, although less pronounced phenotype was also observed in response to  
503 long-term RM treatment (13) (Fig. 7). Despite this seemingly overlapping effect of the two  
504 treatments, the CR- and RM-induced fast-to-slow fiber type conversion was additive in the  
505 forelimb *brachioradialis* muscle of CR+RM treated mice (Fig. 7). Since slower-type fibers are  
506 more resistant to age-related atrophy, the CR-induced fast-to-slow fiber-type transition, despite  
507 the absolute decrease in muscle mass, may ultimately preserve muscle fiber number and  
508 function in aging mice, as previously observed in muscle-specific BDNF knockout mice, which  
509 display a fast-to-slow fiber type transition and increased resistance to age-related muscle  
510 loss(31).

511 A specific feature of CR believed to contribute to its beneficial effects in rodent skeletal  
512 muscle (17) is an increase in physical activity prior to feeding, and may at least partially explain  
513 the fast-to-slow fiber transition. This anticipatory behavior, reminiscent of exercise training, is  
514 not seen in *ad libitum*-fed mice and was not altered by RM in the current study (Fig. 6).  
515 Although the CR-induced quasi exercise training is an artefact of experimental circumstance  
516 not applicable to humans, the combined impact of CR, including any benefits afforded through  
517 behavioral changes were on top of those induced by RM, particularly with regard to slowing of  
518 muscle fiber properties, relative grip strength and voluntary running distance (Fig. 6 & 7). Since  
519 muscle adaptations to exercise are accentuated by protein intake immediately before, during or  
520 after exercise, the close temporal restriction of activity and food intake in CR mice may be  
521 advantageous for maintaining muscle function with age.

522 While together, our experiments clearly demonstrate that the beneficial effects of CR on  
523 muscle do not require mTORC1 suppression and likewise RM treatment is not redundant in

524 restricted mice, the complementary mechanisms allowing the effects of these interventions to  
525 compound are less clear. Both CR and RM are well-known to reduce mTORC1 activity, but  
526 unlike in RM-treated mice, mTORC1 activity still responds to food intake in CR mice, although  
527 its activity is more temporally restricted, and decreases more during fasting periods than in *ad*  
528 *libitum*-fed mice (54). Since transient mTORC1 activity remains important in specific tissues,  
529 most blatantly highlighted by the severe testicular degeneration experienced by RM-treated  
530 mice, it might be expected that CR would represent a more favorable intervention to counter  
531 the detrimentally hyperactive mTORC1 frequently observed in aging tissue. Strikingly, our data  
532 point in the opposite direction, suggesting that CR-induced mTORC1 suppression is not  
533 sufficient to confer all the beneficial effects of RM treatment. Of course, whether this effect  
534 relates directly to muscle tissue mTORC1 suppression or via secondary effects of non-muscle  
535 tissue mTORC1 suppression is unclear.

536 Another explanation for the additive effects of CR and RM, could be co-compensation of  
537 treatment-specific side effects. A prime example relates to glucose tolerance, which is markedly  
538 improved in CR mice (Fig. 1), and impaired by RM (55). However, blood glucose levels were  
539 not habitually high in RM or CR+RM groups, instead, CR+RM-treated mice appeared to curb  
540 the ravenous consumption of daily food allocation seen in CR mice, thereby distributing energy  
541 availability over a prolonged period (Fig. 6K-L). Metabolic analyses showed that this subdued  
542 rate of food intake coincided with a lower RER during the early night-time eating phase but  
543 also a higher RER during the early day-time inactive period in CR+RM compared to CR mice  
544 (Fig. 6J). Whether this smoothing of diurnal fluctuations in energy utilization affords benefits  
545 for CR+RM mice remains to be tested. Along a similar line, we previously reported that specific  
546 muscles respond differently to rapamycin, an effect correlated with the presence (muscle not  
547 protected by RM, i.e. GAS) or absence (muscle protected by RM, i.e. TRI and TA) of pro-  
548 sarcopenic side effects (13). Although a CR-induced amelioration of these negative effects of  
549 RM could explain the combined effects, the same muscle-specific effects of RM were observed

550 in CR+RM mice, with less age-related muscle loss in the TRI and TA, but not in the GAS (Fig.  
551 7A), hinting that further attenuation in muscle aging may be possible beyond combined CR and  
552 RM.

553 Together, our results conclusively demonstrate that CR and RM exert distinct, non-  
554 overlapping and frequently additive effects in aging skeletal muscle. The striking failure of RM  
555 to recapitulate the effects of CR and more surprisingly, the failure of CR to recapitulate the  
556 effects of RM raises the exciting prospect of multiple, additive interventions to counteract  
557 sarcopenia. Further work is needed to systematically isolate targetable processes and examine  
558 the resulting interactions in order to develop optimal strategies to counteract sarcopenia and  
559 promote healthy aging.

560

## 561 **METHODS**

### 562 *Animal care*

563 All procedures were performed in accordance with Swiss regulations for animal  
564 experimentation and approved by the veterinary commission of the Canton Basel-Stadt. Male,  
565 C57BL/6JRj mice for aging studies were purchased from the aging colony at Janvier Labs (Le  
566 Genest-Saint-Isle, France). Transgenic TSCmKO mice and their genotyping were previously  
567 described (33, 56). Littermates floxed for *Tsc1* but not expressing HSA-Cre-recombinase were  
568 used as controls. For all studies, mice were kept in single cages under a fixed 12h light-dark  
569 cycle (6 am to 6 pm) at 22°C (range 20-24°C) and 55% (range 45-65%) relative humidity and  
570 were acclimatized to individual housing and the control diet for 3-4 weeks before the start of  
571 the experiment.

572

### 573 *Aging studies*

574 In the first aging study (results presented in Figures 1-3), two independent groups of mice  
575 were calorie restricted starting at 20 (n=11) or 15 (n=21) months of age. 10mCON, 30mCON

576 and 30mRM data were generated alongside 30mCR, but data from these groups have largely  
577 been previously reported (13). For appropriate interpretation of the previously unreported CR  
578 data, 10mCON and 30mCON data have been included. For combined CR+RM experiments  
579 (Figures 6 and 7), all groups and data were newly generated. After 1-month acclimatization to  
580 individual housing and the standardized AIN-93M diet (TestDiet, 58M1-9GH6) containing 488  
581 ppm Eudragit (Emtora), food intake of CR mice was incrementally reduced to 90%, 80% and  
582 70% for 1 week each before being maintained at 65% of mean baseline food intake. To avoid  
583 malnutrition, the concentration of vitamins and minerals were increased  $1.43 \times$  in CR mice  
584 (58M1-9GH8). Rapamycin treated *ad libitum*-fed and CR mice received an AIN-93M diet  
585 containing 42 or 48  $\text{mg} \cdot \text{kg}^{-1}$  active encapsulated (Eudragit) rapamycin (TestDiet, 58M1-9GH7),  
586 respectively. The concentration of RM was increased in CR+RM mice in an attempt to counter  
587 the discrepancy between body weight ( $\sim 22\%$ ) and food intake reductions ( $-35\%$ ) and deliver  
588 a similar dose of rapamycin per kg body weight. In the week before starting the experiment,  
589 food intake, body mass and composition (via EchoMRI) and grip strength were measured and  
590 used to balance group selection. Each group (CON, CR, RM and CR+RM) contained mice with  
591 an almost identical mean and standard deviation for each measurement within experimental  
592 groups. Food intake and body mass were measured weekly. As previously described (13),  
593 weight gain and obesity was limited in *ad libitum*-fed mice via daily food restriction to that of  
594 the control group mean (3.1 g) in mice with a propensity for overeating and weight gain.

595

### 596 ***TSCmKO studies***

597 Mice were progressively adapted to calorie restriction by incremental reductions in food  
598 intake of 10% per week starting at 12 weeks of age, with mice receiving 70% of the genotype  
599 mean at the start of the 3<sup>rd</sup> week. Baseline food intake was determined over a 3-week period  
600 prior to CR. *Ad libitum*-fed WT and TSCmKO mice ate 3.05 and 3.45  $\text{g} \cdot \text{day}^{-1}$  food, respectively,  
601 under baseline conditions. After CR habituation, WT-CR and TSC-CR groups were



602 therefore given 2.1 and 2.4 g·day<sup>-1</sup> food for 6 months. These experiments were performed over  
603 three separate trials using both female and male mice and either an AIN-93M standardized diet  
604 (D10012M; KLIBA NAFAG) or a standard chow diet (KLIBA NAFAG-3432). Since results  
605 were comparable across all trials, food and sexes, data were pooled for analysis.

606

### 607 ***Body composition analysis***

608 Fat mass and lean mass were measured on restrained, conscious mice using an EchoMRI-  
609 100 (EchoMRI Medical Systems).

610

### 611 ***Whole-body muscle function***

612 Mice were initially familiarized to voluntary running wheels over a 48-72 h period. Mice  
613 were then given free access to voluntary running wheels for a 24 h period every two months in  
614 the first study and once for a 48 h period in the subsequent CR+RM study, with data for the  
615 final 24 h used for analysis. Inverted grid hang time was measured by placing mice on a wire  
616 grid, which was slowly turned upside down and positioned over a ~40 cm high box containing  
617 a foam pad at the bottom. Performance was taken as the longest time a mouse could hold onto  
618 the grip across three trials separated by at least 30 min. All-limb grip strength was measured  
619 using a small grid attached to a force meter (Columbus Instruments). Mice firmly holding the  
620 grid with all four paws were gently pulled horizontally at a consistent speed until the grasp was  
621 broken. Performance was taken as the median of 3-5 trials with at least 10 min rest between  
622 tests. Trials in which the mouse actively pulled on the grid while the test was underway were  
623 discarded. The same researcher performed all grip strength measurements at a similar time of  
624 day.

625

### 626 ***Comprehensive laboratory animal monitoring system (CLAMS)***

627 CLAMS (Columbus Instruments, Columbus, OH) was used to measure whole-body  
628 metabolic parameters including energy expenditure, oxygen consumption ( $\text{VO}_2$ ),  $\text{CO}_2$   
629 production ( $\text{VCO}_2$ ) and the ratio of  $\text{VCO}_2$  to  $\text{VO}_2$  or respiratory exchange ratio (RER), as well  
630 as locomotory activity. RER is dependent on energy substrate utilization, ranging from above  
631 1 to 0.7, which indicates preferential use of carbohydrates and lipids, respectively. Locomotor  
632 activity was measured on X, Y and Z axes using infrared beams. Energy expenditure was  
633 calculated using  $\text{VO}_2$  and RER values and subsequently normalized to body surface area (body  
634 mass<sup>-0.75</sup>) to account for pronounced changes in body size associated with CR. Data were  
635 collected for three consecutive days, with the final 24 h period (6 am to pm) used for analysis.

636

### 637 *In vitro muscle force*

638 *In vitro* muscle force was measured in the fast-twitch *extensor digitorum longus* (EDL) and  
639 slow-twitch *soleus* muscles. After careful isolation, muscle tendons were tied with surgical  
640 suture at each end and mounted on the 1200A Isolated Muscle System (Aurora Scientific,  
641 Aurora, ON, Canada) in an organ bath containing 60 mL of Ringer solution (137 mM NaCl, 24  
642 mM  $\text{NaHCO}_3$ , 11 mM Glucose, 5 mM KCl, 2 mM  $\text{CaCl}_2$ , 1 mM  $\text{MgSO}_4$ , 1 mM  $\text{NaH}_2\text{PO}_4$ )  
643 gassed with 95%  $\text{O}_2$ ; 5%  $\text{CO}_2$  at 30 °C. After defining optimal length, muscles were stimulated  
644 with 15 V pulses. Muscle force was recorded in response to 500 ms pulses of 10-250 Hz. Muscle  
645 fatigue was assessed by 6 min of repeated tetanic stimulations at 200 Hz for EDL and 120 Hz  
646 for SOL, respectively, separated by 8 sec.

647

### 648 *Immunostaining of muscle cross sections*

649 Muscles were mounted at resting length in optimal cutting temperature medium (O.C.T,  
650 Tissue-Tek) and snap-frozen in thawing isopentane for ~1 min before transfer to liquid nitrogen  
651 and storage at -80°C. Muscle sections (10  $\mu\text{m}$ ) were cut from the mid belly at -20° C on a  
652 cryostat (Leica, CM1950), collected on SuperFrost Plus (VWR) adhesion slides and stored at -

653 80° C. Sections from each experimental condition were always mounted on the same slide to  
654 ensure accurate comparisons. For fiber typing, sections were blocked and permeabilized in PBS  
655 containing 10% goat serum and 0.4% triton X-100 for 30 min before being incubated for 2 h at  
656 RT in a primary antibody solution containing BA-D5, SC-71, BF-F3 which were developed by  
657 Prof. Stefano Schiaffino and obtained from the Developmental Studies Hybridoma Bank  
658 developed under the auspices of the National Institute of Child Health and Human Development  
659 and maintained by the University of Iowa Department of Biology as well as laminin (#11575;  
660 Abcam) and 10% goat serum. After incubation in primary antibodies, sections were washed 4  
661 × 10 min in PBS and then incubated in a secondary antibody solution containing DyLight 405  
662 (#115-475-207, Jackson), Alexa568 (#A-21124, Invitrogen), Alexa488 (#A-21042,  
663 Invitrogen), Alexa647 (#711-605-152, Jackson) and 10% goat serum. Sections were then  
664 washed 4 × 10 min in PBS and mounted with ProLong™ Gold antifade (Invitrogen). Muscle  
665 sections were imaged at the Biozentrum Imaging Core Facility with an Axio Scan.Z1 Slide  
666 Scanner (Zeiss) equipped with appropriate band-pass filters. Fiji macros were developed in-  
667 house to allow an automated analysis of muscle fiber types (based on intensity thresholds) and  
668 muscle cross-sectional area (i.e., minimal Feret's diameter; based on cell segmentation) (31).  
669 All macros and scripts used in this study are available upon request. For P62 staining, TA  
670 sections were thawed for 10 min at RT, fixed in 4% PFA for 6min, neutralized in 0.1M Glycine  
671 (pH7.4) at RT for 2 × 15 min and then blocked at RT for 1.5 h in blocking solution containing  
672 3% IgG free Bovine Serum Albumin (BSA), 1% Fab anti-mouse IgG (Jackson) and 0.25%  
673 Triton-X. Slides were then incubated in primary antibody solution containing P62 (GP62-C,  
674 1:300), laminin (ab11576, Jackson 1:300) and 3% BSA overnight at 4°C. The next day, slides  
675 were washed 3 × 10 min in PBS and incubated in secondary antibody solution containing DaGP  
676 Cy3 (706-165-148; Jackson; 1:500) and GaRt 488 (112-545-003, Jackson; 1:500) for 1.5h at  
677 RT. Afterwards, sections were washed 2 × 10 min in PBS and mounted with Vectashield DAPI  
678 (Vector Laboratories).

679

680 ***Protein extraction and Western blot analysis***

681 For TSC-CR studies, TA and GAS muscles were snap-frozen, pulverized in liquid nitrogen  
682 and lysed in RIPA buffer before sonication and 2 h incubation at 4° C. Lysates were then  
683 centrifuged at 16,000 g for 30 min at 4° C to remove insoluble material. Protein concentration  
684 was measured (BCA assay) and normalized with RIPA buffer before being heated for 5 min at  
685 95° C in Laemmli buffer (0.1 M Tris-HCl pH 6.8, 10% Glycerol, 2% SDS, 0.04%  
686 Bromphenolblue, 1% β-mercaptoethanol). Proteins were separated on 4-12% Bis-Tris protein  
687 gels (NuPAGE, Life Technologies) and transferred onto nitrocellulose membranes. Membranes  
688 were blocked for 1 h at RT in 3% BSA in TBS containing 0.1% Tween20 and incubated  
689 overnight with primary antibodies in blocking solution at 4° C. The next day, membranes were  
690 washed 3 × 10 min in TBS before incubation in secondary horseradish peroxidase-conjugated  
691 antibodies, diluted in blocking solution. Membranes were then washed 3 × 10 min in TBS  
692 before immunoreactivity was visualized using the KLP LumiGlo Chemiluminescence Substrate  
693 Kit (Seracare) with a Fusion Fx machine (Vilber). Protein abundance was quantified using  
694 FusionCapt Advance (Vilber) as mean grey value minus background and then normalized to a  
695 housekeeping protein. Western blots for all proteins were performed on TA muscle. For key  
696 proteins (phospho and total mTOR, S6, 4EBP1 and AKT, as well as P62 and LC3B), western  
697 blots were also performed on GAS muscle. Results in both muscles were comparable and were  
698 subsequently averaged for each mouse for further analysis. All primary antibodies were from  
699 Cell Signaling Technology: p<sup>S2448</sup>mTOR (#2971), mTOR (#2972), p<sup>S240/244</sup>S6 (#5364),  
700 p<sup>S235/236</sup>S6 (#2211), S6 (#2217), p<sup>S65</sup>4EBP1 (#9451), 4EBP1 (#9452), LC3B (#2775), p<sup>S757</sup>ULK  
701 (#6888), ULK (#8054), Beclin1 (#3495), Bnip3 (#3769), p<sup>T246</sup>PRAS40 (#2997), PRAS40  
702 (#2610), p<sup>S473</sup>AKT (#4058), AKT (#9272) and BiP (#3177) at a dilution of 1:1000, except  
703 ATF4 (sc-200, Santa Cruz, 1:1000), FGF21 (AF3057, 1:500), α-actinin (A7732, Sigma,  
704 1:5000) and P62 (GP62-C, Pro-Gene, 1:1000).

705

706 ***RT-qPCR***

707 Snap frozen gastrocnemius muscles were pulverized and lysed in RLT buffer (Qiagen).  
708 RNA was extracted using the RNeasy® Mini Kit (Qiagen), with Proteinase K and DNase  
709 treatment, according to the supplier's instructions. RNA purity was determined using a  
710 Nanodrop ONEC (Thermo Scientific). cDNA was generated with the iScript™ cDNA  
711 Synthesis Kit (Bio-Rad) using 500 ng of extracted RNA according to supplier's manual. cDNA  
712 samples were stored at -20°C. RT-qPCR was performed in duplicate with the LightCycler 480  
713 (Roche Diagnostics) instrument using LightCycler 384-well plates with sealing foil (Roche).  
714 The reaction volume of 10 µl contained, FastStart Essential DNA Green Master Mix (2X,  
715 Roche), forward and reverse primers and cDNA template (1:5 diluted). Primers were designed  
716 using Genious®10 software (57) and specificity confirmed by the Basic Local Alignment  
717 Search Tool (BLAST) (58). Potential hairpin formation, complementarity and self-annealing  
718 sites were verified to be negative by OligoCalc (59). The amplification of a single PCR product  
719 was confirmed with a melting-point dissociation curve and raw quantification cycle (Cq) values  
720 were calculated by a LightCycler 480. Data were analyzed using the comparative Cq method  
721 ( $2^{-\Delta\Delta Cq}$ ). Raw Cq values of target genes were normalized to Cq values of a housekeeping gene  
722 ( $\beta$ -actin), which was stable between conditions, and then further normalized to the control group  
723 for ease of visualization. Primers used are as follows:

724 *Map11c3a*: Fwd-GTTGGATGTGTTCTGTCTCGTCAC; Rev-

725 CTACGTGATTATTTCCGTGTTGCT

726 *Atg7*: Fwd-TGCAGTTCGCCCCCTTTAAT; Rev-CAGGCGGTACTCGTTCAACT

727 *Bnip3*: Fwd-TTCCACTAGCACCTTCTGATGA; Rev-GAACACCGCATTACAGAACAA

728 *Gabarapl1*: Fwd-CATCGTGGAGAAGGCTCCTA; Rev-ATACAGCTGGCCCATGGTAG

729 *Sqstm1*: Fwd-TACTCGAACGACACAAGGGA; Rev-GACTCAGCTGTAGGGCAAGG

730 *Ctsl*: Fwd-GTGGACTGTTCTCACGCTCA; Rev-TCCGTCCTTCGCTTCATAGG

731 *Trib3*: Fwd-GGACAAGATGCGAGCCACAT; Rev-CCACAGCAGGTGACAAGTCT  
732 *Xbp1*: Fwd-TGGCCGGGTCTGCTGAGTCCG; Rev-GTCCATGGGAAGATGTTCTGG  
733 *Keap1*: Fwd-GGCAGGACCAGTTGAACAGT; Rev-GGGTCACCTCACTCCAGGTA  
734 *Gstal*: Fwd-CCAGAGCCATTCTCAACTA; Rev-TGCCCAATCATTTCAGTCAG

735

### 736 ***RNA extraction for aging-calorie restriction data sets***

737 For the aging-CR-RM data set, RNA extraction was performed as previously described in  
738 detail (13). Briefly, TA, TRI, GAS and SOL muscles from 6 mice per group were pulverized  
739 and lysed in RLT buffer (Qiagen) and treated with proteinase K (Qiagen) and DNase. RNA  
740 was extracted with an iColumn 24 (AccuBioMed) with an AccuPure Tissue RNA Mini Kit  
741 (AccuBioMed). RNA purity and integrity was examined with a Bioanalyser (Agilent). RNA  
742 concentration was determined with a Quant-iT™ RiboGreen™ RNA assay kit and Qubit  
743 flurometer (Invitrogen). Libraries were prepared with TruSeq Stranded mRNA HT Sample Prep  
744 Kit. Stranded, paired-end sequencing with 101 base pair read length was performed on an  
745 Illumina HiSeq2500 platform. A single outlier in the 30mCON SOL group was identified and  
746 removed from further analysis based on a clear technical error.

747

### 748 ***Statistical analysis***

749 All values are expressed as mean ± SEM unless stated otherwise. Data were tested for  
750 normality and homogeneity of variance using a Shapiro-Wilk and Levene's test, respectively.  
751 Data were analysed in GraphPad Prism 8. Student t-tests were used for pairwise comparisons,  
752 while one-way ANOVAs with Fisher's LSD post hoc tests were used to compare between three  
753 groups, so long as the ANOVA reached statistical significance. Two-way ANOVAs or two-  
754 way repeated measures ANOVAs for multiple recordings over time, with Sidak or Tukeys post  
755 hoc tests were used to compare between groups with two independent variables. Both  
756 significant differences ( $P < 0.05$ ) and trends ( $P < 0.1$ ) are reported where appropriate.

757

## 758 *RNA-Seq data processing*

759 Paired-end RNA-Seq reads were subjected to 3' adapter (mate 1 5'-  
760 AGATCGGAAGAGCACACGTC-3', mate 2 5'-AGATCGGAAGAGCGTCGTGT-3') and  
761 poly(A)/poly(T) trimming using Cutadapt v1.9.1 (60). Reads shorter than 30 nucleotides were  
762 discarded. As the reference transcriptome, we considered sequences of protein-coding  
763 transcripts with support level 1-3 based on the genome assembly GRCm38 (release 92) for  
764 mouse and corresponding transcript annotations from Ensembl database (61). The kallisto  
765 v0.43.1 software was used to assign filtered reads to mouse transcriptome (62). The default  
766 options of kallisto were utilized for building the transcriptome index. For aligning stranded  
767 RNA-Seq reads, where mates 1 and 2 originated from antisense and sense strands, respectively,  
768 the option '--rf-stranded' was used. The option '--pseudobam' was used to save kallisto  
769 pseudoalignments to a BAM file.

770 Mapped reads were then assigned to transcripts in a weighted manner: if a read was  
771 uniquely mapped to a transcript, then the transcript's read count was incremented by 1; if a read  
772 was mapped to  $n$  different transcripts, each transcript's read count was incremented by  $1/n$ .  
773 Trimming 3' adapters and poly(A)/poly(T) stretches, indexing reference transcriptomes,  
774 mapping the RNA-Seq reads to transcripts and counting reads assigned to individual transcripts  
775 were performed with a Snakemake framework (63).

776 The expression of each transcript  $t_i$  was then estimated in units of transcripts per million  
777 (TPM) by dividing the read count  $c_i$  corresponding to the transcript by the transcript length  $l_i$   
778 and normalizing to the library size:

$$779 \quad t_i = \frac{\frac{c_i}{l_i}}{\sum_{j=1}^{\# \text{ of transcripts}} \frac{c_j}{l_j}} \cdot 10^6.$$

780 The expression level of a gene was calculated as the sum of normalized expression levels  
781 of transcripts associated with the gene. For every gene, read counts of transcripts associated  
782 with this gene were also summed up.

783

#### 784 *Calculating log-fold changes in the gene expression across conditions*

785 Calculating log-fold changes in the gene expression across conditions was performed with  
786 EdgeR available through the R/Bioconductor package (64). A gene was included in the analysis  
787 only if it had at least 1 count per million (CPM) in the number of samples corresponding to the  
788 minimum number of replicates of the same condition across conditions. Obtained log-fold  
789 changes were subjected to the hierarchical clustering based on Euclidean distance.

790

#### 791 *Aligning gene expression with principal components*

792 The gene expression matrix with samples as columns and log<sub>2</sub>-transformed gene  
793 expression in TPM units as rows was mean centered to make the data comparable both across  
794 samples and genes. The centered gene expression matrix was further subjected to the principal  
795 component analysis (PCA). First four principal components, PC1, PC2, PC3 and PC4, were  
796 defined for each data subset, respectively. Then for each data subset we quantified how much  
797 individual genes contributed to the corresponding principal component (13). Shortly, we  
798 represented genes in the multi-dimensional sample space, localized principal components and  
799 calculated projections of vectors associated with genes on principal components and  
800 correlations between gene vectors and principal components. We considered a projection of the  
801 gene vector on PC significant if its absolute *z*-score value was  $\geq 1.96$ . The correlation between  
802 a gene vector and PC was considered as significant if the absolute value was  $\geq 0.4$ .

803

#### 804 *Gene Set Enrichment Analysis*



805 The distribution of gene sets in ranked gene lists was examined using GSEA(65). Ranking  
806 was based on log-fold changes in the gene expression between two conditions of interest.  
807 Enrichment was considered significant if FDR was less than 0.01.

808

### 809 *Hierarchical Clustering*

810 Hierarchical clustering of genes was based on Euclidean distance between changes in the  
811 gene expression in notified conditions (see Fig. 3E).

812

### 813 *Gene ontology analysis*

814 To annotate genes aligned with PCs, we performed the gene ontology (GO) analysis using  
815 Database for Annotation, Visualization and Integrated Discovery (DAVID) (66) through the  
816 R/Bioconductor package called ‘RDAVIDWebService’ (67). ‘GOTERM\_BP\_DIRECT’,  
817 ‘GOTERM\_MF\_DIRECT’ and ‘GOTERM\_CC\_DIRECT’ categories were used for gene  
818 annotation. Background genes for calculating enrichment statistics consisted of all genes  
819 expressed in muscle samples (see the section ‘Aligning gene expression with principal  
820 components’). GO terms with a p-value less than 0.01 were considered significantly enriched.

821

### 822 *Shiny application*

823 To make CR high-throughput data set and data analysis tools available for the research  
824 community, we included them in the previously developed interactive web application  
825 ‘SarcoAtlas’ based on the R package Shiny (version 0.14.2, [https://cran.r-](https://cran.r-project.org/web/packages/shiny/index.html)  
826 [project.org/web/packages/shiny/index.html](https://cran.r-project.org/web/packages/shiny/index.html)). The application supports gene expression  
827 plotting, differential expression analysis, principal component analysis and aligning gene  
828 expression with principal components. Moreover, the application can submit genes resulting  
829 from the analysis to STRING (68) to further investigate protein-protein interactions and

830 perform GO analysis. The application can be accessed through the following link:

831 <https://sarcoatlas.scicore.unibas.ch/> [10].

832

833

834 **References**

- 835 1. J. Most, V. Tosti, L. M. Redman, L. Fontana, Calorie restriction in humans: An  
836 update. *Ageing Res Rev* **39**, 36-45 (2017).
- 837 2. A. W. McCracken, G. Adams, L. Hartshorne, M. Tatar, M. J. P. Simons, The hidden  
838 costs of dietary restriction: Implications for its evolutionary and mechanistic origins.  
839 *Sci Adv* **6**, eaay3047 (2020).
- 840 3. L. Fontana, L. Partridge, Promoting health and longevity through diet: from model  
841 organisms to humans. *Cell* **161**, 106-118 (2015).
- 842 4. R. W. Powers, 3rd, M. Kaeberlein, S. D. Caldwell, B. K. Kennedy, S. Fields,  
843 Extension of chronological life span in yeast by decreased TOR pathway signaling.  
844 *Genes Dev* **20**, 174-184 (2006).
- 845 5. I. Bjedov *et al.*, Mechanisms of life span extension by rapamycin in the fruit fly  
846 *Drosophila melanogaster*. *Cell Metab* **11**, 35-46 (2010).
- 847 6. S. Robida-Stubbs *et al.*, TOR signaling and rapamycin influence longevity by  
848 regulating SKN-1/Nrf and DAF-16/FoxO. *Cell Metab* **15**, 713-724 (2012).
- 849 7. D. E. Harrison *et al.*, Rapamycin fed late in life extends lifespan in genetically  
850 heterogeneous mice. *Nature* **460**, 392-395 (2009).
- 851 8. A. Unnikrishnan, K. Kurup, A. B. Salmon, A. Richardson, Is Rapamycin a Dietary  
852 Restriction Mimetic? *J Gerontol A Biol Sci Med Sci* **75**, 4-13 (2020).
- 853 9. WHO, "Decade of healthy ageing: baseline report," (World Health Organization,  
854 Geneva, 2020).
- 855 10. S. C. Bodine *et al.*, Akt/mTOR pathway is a crucial regulator of skeletal muscle  
856 hypertrophy and can prevent muscle atrophy in vivo. *Nat Cell Biol* **3**, 1014-1019  
857 (2001).
- 858 11. T. Moro, S. M. Ebert, C. M. Adams, B. B. Rasmussen, Amino Acid Sensing in  
859 Skeletal Muscle. *Trends in endocrinology and metabolism: TEM* **27**, 796-806 (2016).

- 860 12. G. Stallone, B. Infante, C. Prisciandaro, G. Grandaliano, mTOR and Aging: An Old  
861 Fashioned Dress. *Int J Mol Sci* **20**, (2019).
- 862 13. D. J. Ham *et al.*, The neuromuscular junction is a focal point of mTORC1 signaling in  
863 sarcopenia. *Nat Commun* **11**, 4510 (2020).
- 864 14. A. Borsch *et al.*, Molecular and phenotypic analysis of rodent models reveals  
865 conserved and species-specific modulators of human sarcopenia. *Commun Biol* **4**, 194  
866 (2021).
- 867 15. G. Valdez *et al.*, Attenuation of age-related changes in mouse neuromuscular synapses  
868 by caloric restriction and exercise. *Proc Natl Acad Sci U S A* **107**, 14863-14868  
869 (2010).
- 870 16. Y. C. Jang *et al.*, Dietary restriction attenuates age-associated muscle atrophy by  
871 lowering oxidative stress in mice even in complete absence of CuZnSOD. *Aging Cell*  
872 **11**, 770-782 (2012).
- 873 17. K. van Norren *et al.*, Behavioural changes are a major contributing factor in the  
874 reduction of sarcopenia in caloric-restricted ageing mice. *J Cachexia Sarcopenia*  
875 *Muscle* **6**, 253-268 (2015).
- 876 18. L. M. Margolis *et al.*, Prolonged Calorie Restriction Downregulates Skeletal Muscle  
877 mTORC1 Signaling Independent of Dietary Protein Intake and Associated microRNA  
878 Expression. *Front Physiol* **7**, 445 (2016).
- 879 19. W. C. Fok *et al.*, Short-term treatment with rapamycin and dietary restriction have  
880 overlapping and distinctive effects in young mice. *J Gerontol A Biol Sci Med Sci* **68**,  
881 108-116 (2013).
- 882 20. V. P. Houde *et al.*, Chronic rapamycin treatment causes glucose intolerance and  
883 hyperlipidemia by upregulating hepatic gluconeogenesis and impairing lipid  
884 deposition in adipose tissue. *Diabetes* **59**, 1338-1348 (2010).

- 885 21. W. C. Fok *et al.*, Combined treatment of rapamycin and dietary restriction has a larger  
886 effect on the transcriptome and metabolome of liver. *Aging Cell* **13**, 311-319 (2014).
- 887 22. P. P. Karunadharma *et al.*, Subacute calorie restriction and rapamycin discordantly  
888 alter mouse liver proteome homeostasis and reverse aging effects. *Aging Cell* **14**, 547-  
889 557 (2015).
- 890 23. S. E. Mitchell *et al.*, The effects of graded levels of calorie restriction: I. impact of  
891 short term calorie and protein restriction on body composition in the C57BL/6 mouse.  
892 *Oncotarget* **6**, 15902-15930 (2015).
- 893 24. S. E. Mitchell *et al.*, The effects of graded levels of calorie restriction: III. Impact of  
894 short term calorie and protein restriction on mean daily body temperature and torpor  
895 use in the C57BL/6 mouse. *Oncotarget* **6**, 18314-18337 (2015).
- 896 25. T. H. Reynolds *et al.*, The impact of age and sex on body composition and glucose  
897 sensitivity in C57BL/6J mice. *Physiol Rep* **7**, e13995 (2019).
- 898 26. M. Guridi *et al.*, Activation of mTORC1 in skeletal muscle regulates whole-body  
899 metabolism through FGF21. *Sci Signal* **8**, ra113 (2015).
- 900 27. G. A. Joseph *et al.*, Partial inhibition of mTORC1 in aged rats counteracts the decline  
901 in muscle mass and reverses molecular signaling associated with sarcopenia. *Mol Cell*  
902 *Biol*, (2019).
- 903 28. E. L. Baar, K. A. Carbajal, I. M. Ong, D. W. Lamming, Sex- and tissue-specific  
904 changes in mTOR signaling with age in C57BL/6J mice. *Aging Cell* **15**, 155-166  
905 (2016).
- 906 29. H. Tang *et al.*, mTORC1 underlies age-related muscle fiber damage and loss by  
907 inducing oxidative stress and catabolism. *Aging Cell* **18**, e12943 (2019).
- 908 30. B. Conti, Considerations on temperature, longevity and aging. *Cell Mol Life Sci* **65**,  
909 1626-1630 (2008).

- 910 31. J. Delezie *et al.*, BDNF is a mediator of glycolytic fiber-type specification in mouse  
911 skeletal muscle. *Proc Natl Acad Sci U S A* **116**, 16111-16120 (2019).
- 912 32. M. V. Blagosklonny, Calorie restriction: decelerating mTOR-driven aging from cells  
913 to organisms (including humans). *Cell Cycle* **9**, 683-688 (2010).
- 914 33. P. Castets *et al.*, Sustained activation of mTORC1 in skeletal muscle inhibits  
915 constitutive and starvation-induced autophagy and causes a severe, late-onset  
916 myopathy. *Cell Metab* **17**, 731-744 (2013).
- 917 34. Z. White, R. B. White, C. McMahon, M. D. Grounds, T. Shavlakadze, High mTORC1  
918 signaling is maintained, while protein degradation pathways are perturbed in old  
919 murine skeletal muscles in the fasted state. *Int J Biochem Cell Biol* **78**, 10-21 (2016).
- 920 35. S. H. Um *et al.*, Absence of S6K1 protects against age- and diet-induced obesity while  
921 enhancing insulin sensitivity. *Nature* **431**, 200-205 (2004).
- 922 36. A. H. Lee, N. N. Iwakoshi, L. H. Glimcher, XBP-1 regulates a subset of endoplasmic  
923 reticulum resident chaperone genes in the unfolded protein response. *Mol Cell Biol* **23**,  
924 7448-7459 (2003).
- 925 37. M. Dodson, M. Redmann, N. S. Rajasekaran, V. Darley-Usmar, J. Zhang, KEAP1-  
926 NRF2 signalling and autophagy in protection against oxidative and reductive  
927 proteotoxicity. *Biochem J* **469**, 347-355 (2015).
- 928 38. T. B. Kirkwood, D. P. Shanley, Food restriction, evolution and ageing. *Mech Ageing*  
929 *Dev* **126**, 1011-1016 (2005).
- 930 39. D. P. Shanley, T. B. Kirkwood, Calorie restriction and aging: a life-history analysis.  
931 *Evolution* **54**, 740-750 (2000).
- 932 40. C. K. Lee, R. G. Klopp, R. Weindruch, T. A. Prolla, Gene expression profile of aging  
933 and its retardation by caloric restriction. *Science* **285**, 1390-1393 (1999).
- 934 41. T. B. Kirkwood, S. N. Austad, Why do we age? *Nature* **408**, 233-238 (2000).

- 935 42. K. Giller *et al.*, Beneficial effects of a 6-month dietary restriction are time-dependently  
936 abolished within 2 weeks or 6 months of refeeding-genome-wide transcriptome  
937 analysis in mouse liver. *Free Radic Biol Med* **61**, 170-178 (2013).
- 938 43. J. Most, L. M. Redman, Impact of calorie restriction on energy metabolism in humans.  
939 *Exp Gerontol* **133**, 110875 (2020).
- 940 44. R. S. Sohal, M. J. Forster, Caloric restriction and the aging process: a critique. *Free*  
941 *Radic Biol Med* **73**, 366-382 (2014).
- 942 45. L. M. Redman *et al.*, Metabolic Slowing and Reduced Oxidative Damage with  
943 Sustained Caloric Restriction Support the Rate of Living and Oxidative Damage  
944 Theories of Aging. *Cell Metab* **27**, 805-815 e804 (2018).
- 945 46. D. A. Sinclair, Toward a unified theory of caloric restriction and longevity regulation.  
946 *Mech Ageing Dev* **126**, 987-1002 (2005).
- 947 47. P. M. Gordon *et al.*, Resistance exercise training influences skeletal muscle immune  
948 activation: a microarray analysis. *J Appl Physiol (1985)* **112**, 443-453 (2012).
- 949 48. S. H. Lecker *et al.*, Multiple types of skeletal muscle atrophy involve a common  
950 program of changes in gene expression. *FASEB J* **18**, 39-51 (2004).
- 951 49. C. Ibebunjo *et al.*, Genomic and proteomic profiling reveals reduced mitochondrial  
952 function and disruption of the neuromuscular junction driving rat sarcopenia. *Mol Cell*  
953 *Biol* **33**, 194-212 (2013).
- 954 50. J. Zhou, Z. Liao, J. Chen, K. Zhao, Q. Xiao, Integrated study on comparative  
955 transcriptome and skeletal muscle function in aged rats. *Mech Ageing Dev* **169**, 32-39  
956 (2018).
- 957 51. C. Y. Ewald, J. N. Landis, J. Porter Abate, C. T. Murphy, T. K. Blackwell, Dauer-  
958 independent insulin/IGF-1-signalling implicates collagen remodelling in longevity.  
959 *Nature* **519**, 97-101 (2015).

- 960 52. Y. L. Chen *et al.*, Adiponectin receptor PAQR-2 signaling senses low temperature to  
961 promote *C. elegans* longevity by regulating autophagy. *Nat Commun* **10**, 2602 (2019).
- 962 53. B. Schumacher *et al.*, Delayed and accelerated aging share common longevity  
963 assurance mechanisms. *PLoS Genet* **4**, e1000161 (2008).
- 964 54. R. Tulsian, N. Velingkaar, R. Kondratov, Caloric restriction effects on liver mTOR  
965 signaling are time-of-day dependent. *Aging (Albany NY)* **10**, 1640-1648 (2018).
- 966 55. D. W. Lamming *et al.*, Rapamycin-induced insulin resistance is mediated by mTORC2  
967 loss and uncoupled from longevity. *Science* **335**, 1638-1643 (2012).
- 968 56. D. J. Kwiatkowski *et al.*, A mouse model of TSC1 reveals sex-dependent lethality  
969 from liver hemangiomas, and up-regulation of p70S6 kinase activity in Tsc1 null cells.  
970 *Hum Mol Genet* **11**, 525-534 (2002).
- 971 57. M. Kearse *et al.*, Geneious Basic: an integrated and extendable desktop software  
972 platform for the organization and analysis of sequence data. *Bioinformatics* **28**, 1647-  
973 1649 (2012).
- 974 58. S. F. Altschul, W. Gish, W. Miller, E. W. Myers, D. J. Lipman, Basic local alignment  
975 search tool. *J Mol Biol* **215**, 403-410 (1990).
- 976 59. W. A. Kibbe, OligoCalc: an online oligonucleotide properties calculator. *Nucleic  
977 Acids Res* **35**, W43-46 (2007).
- 978 60. M. Martin, Cutadapt removes adapter sequences from high-throughput sequencing  
979 reads. *EMBnet.journal* **17**, 10-12 (2011).
- 980 61. T. Hubbard *et al.*, The Ensembl genome database project. *Nucleic Acids Res* **30**, 38-41  
981 (2002).
- 982 62. N. L. Bray, H. Pimentel, P. Melsted, L. Pachter, Near-optimal probabilistic RNA-seq  
983 quantification. *Nat Biotechnol* **34**, 525-527 (2016).
- 984 63. J. Koster, S. Rahmann, Snakemake-a scalable bioinformatics workflow engine.  
985 *Bioinformatics* **34**, 3600 (2018).



- 986 64. S. Durinck, P. T. Spellman, E. Birney, W. Huber, Mapping identifiers for the  
987 integration of genomic datasets with the R/Bioconductor package biomaRt. *Nat Protoc*  
988 **4**, 1184-1191 (2009).
- 989 65. A. Subramanian *et al.*, Gene set enrichment analysis: a knowledge-based approach for  
990 interpreting genome-wide expression profiles. *Proc Natl Acad Sci U S A* **102**, 15545-  
991 15550 (2005).
- 992 66. W. Huang da, B. T. Sherman, R. A. Lempicki, Systematic and integrative analysis of  
993 large gene lists using DAVID bioinformatics resources. *Nat Protoc* **4**, 44-57 (2009).
- 994 67. C. Fresno, E. A. Fernandez, RDAVIDWebService: a versatile R interface to DAVID.  
995 *Bioinformatics* **29**, 2810-2811 (2013).
- 996 68. B. Snel, G. Lehmann, P. Bork, M. A. Huynen, STRING: a web-server to retrieve and  
997 display the repeatedly occurring neighbourhood of a gene. *Nucleic Acids Res* **28**,  
998 3442-3444 (2000).
- 999 69. T. Barrett *et al.*, NCBI GEO: archive for high-throughput functional genomic data.  
1000 *Nucleic Acids Res* **37**, D885-890 (2009).

1001

1002

1003 **Acknowledgements**

1004 We gratefully acknowledge Dr. Mikhail Pachkov for help with data processing, Dr. Alexander  
1005 Kanitz for testing and Pablo Escobar López for publishing SarcoAtlas and Dr. Erik van  
1006 Nimwegen for fruitful discussions about data analysis. We also acknowledge the support of the  
1007 University of Basel's Quantitative Genomics Facility, in particular Phillippe Demougin for  
1008 assistance with mRNA-seq sample preparation; the Image Core Facility, in particular Kai  
1009 Schleicher and; the scientific computing center, sciCORE (<http://scicore.unibas.ch/>), where  
1010 calculations were performed.

1011

1012 **Funding**

1013 This work was financially supported by the Cantons of Basel-Stadt and Basel-landschaft, a  
1014 Jubiläumsstiftung from Swiss Life awarded to N.M., and a Sinergia grant (CRSII3\_160760)  
1015 from the Swiss National Science Foundation awarded to M. A.R., M. Z. and C.H.

1016

1017 **Author contributions**

1018 Conceptualization: DJH, NM, MAR, MZ, AB, LAT

1019 Methodology: DJH, NM, KC, SL, LAT, AB

1020 Investigation: DJH, NM, KC, SL, ABL, ASH, RF, MT, JD, LAT, DB

1021 Data curation and formal analysis: AB, DJH

1022 Statistical analysis: DJH, AB

1023 Software: AB

1024 Visualization: DJH, AB

1025 Supervision: MAR, MZ

1026 Writing-original draft: DJH, AB, MAR

1027 Writing-review and editing: DJH, MAR, NM, AB, MZ, LT

1028 Funding Acquisition: MAR, MZ, NM, CH, MS

1029 **Competing interests**

1030 The authors declare that they have no competing interests.

1031

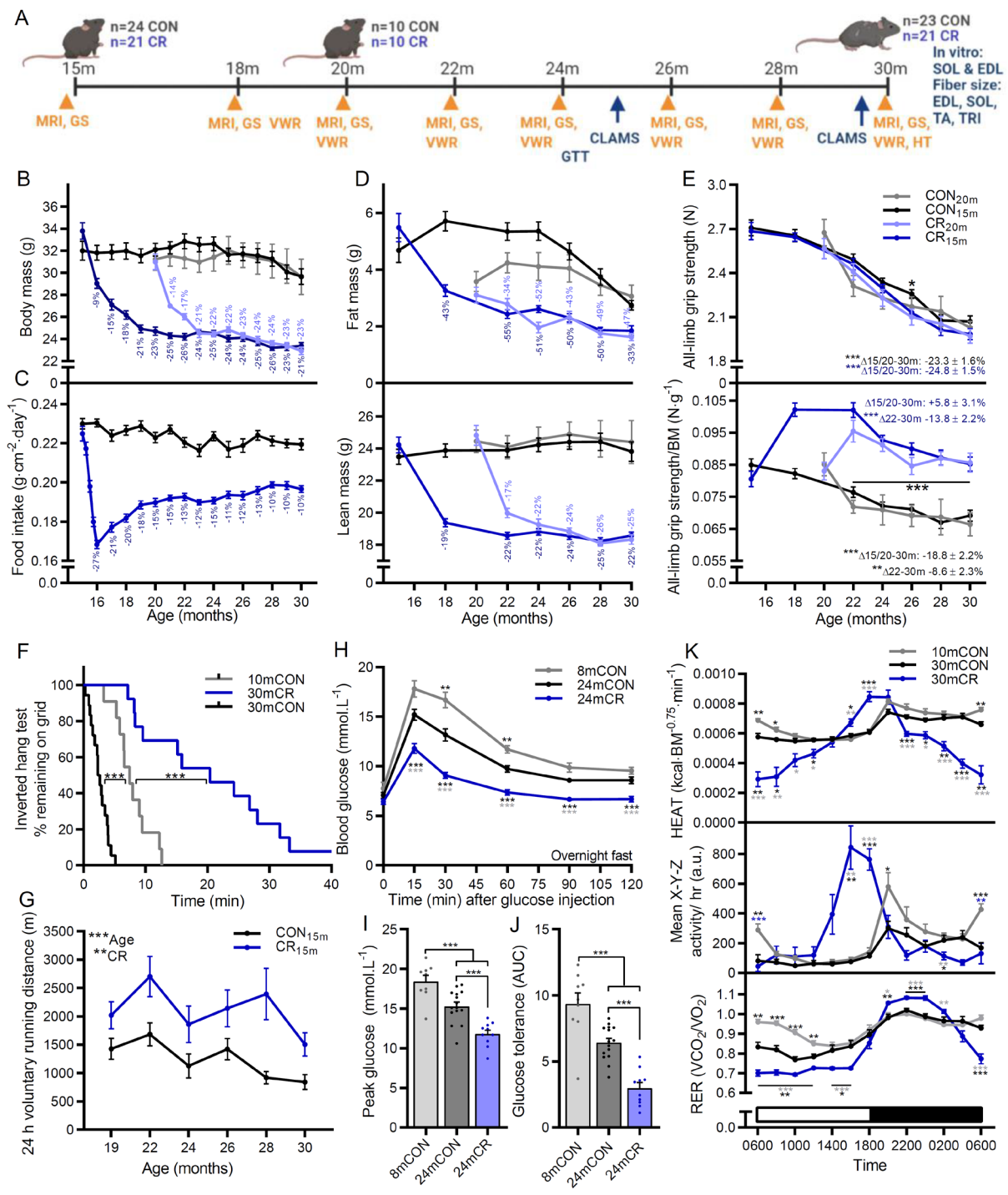
1032 **Data and materials availability**

1033 RNA-Seq data set on four muscles (GAS, TA, TRI and SOL) from six 30-month-old  
1034 calorie restricted mice was deposited to Gene Expression Omnibus (GEO,  
1035 <https://www.ncbi.nlm.nih.gov/geo/>) (69) under the accession number GSE171322. RNA-Seq  
1036 data describing profiles of four muscles (GAS, TA, TRI and SOL) of 10-month-old, 30-month-  
1037 old and 30-month-old mice treated with rapamycin were previously published (13) and  
1038 available at GEO under the accession number GSE139204. These data are also accessible using  
1039 the web-based application, SarcoAtlas (<https://sarcoatlas.scicore.unibas.ch/>). Code is available  
1040 upon request.

1041

1042

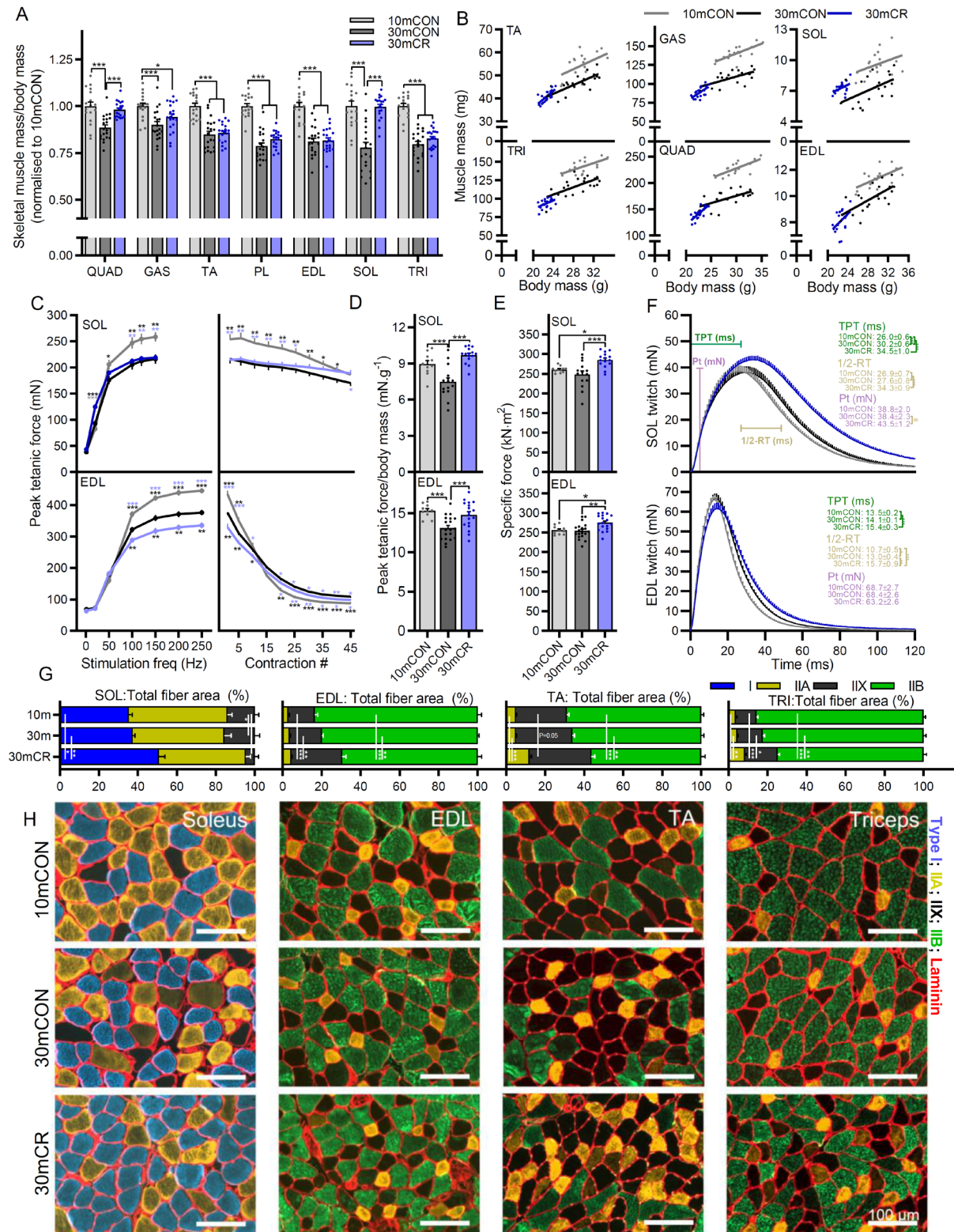
1043 **Figure 1**



1045 **Figure 1: CR promotes beneficial metabolic and functional adaptations but does not**  
1046 **prevent the age-related loss of muscle function. (A)** Experimental design schematic showing  
1047 start and endpoints of middle and late intervention groups as well as time course of  
1048 physiological measures including body composition (MRI), grip strength (GS), voluntary wheel  
1049 running (VWR), whole-body metabolism (CLAMS), hang test (HT) and glucose tolerance test  
1050 (GTT). **(B)** Body mass for mouse groups fed *ad libitum* or 65% of *ad libitum* beginning at 15  
1051 months (CON<sub>15m</sub> and CR<sub>15m</sub>) or 20 months (CON<sub>20m</sub> and CR<sub>20m</sub>) of age. **(C)** Mean daily food  
1052 intake normalized to body surface area for middle-aged groups. **(D)** Bimonthly recordings of  
1053 whole-body fat (upper) and lean mass (lower);  $n = 18$  (CON<sub>15m</sub>), 13 (CR<sub>15m</sub>), 6 (CON<sub>20m</sub>), and  
1054 8 (CR<sub>20m</sub>) mice. **(E)** absolute (upper) and body mass normalized (lower) all-limb grip  
1055 strength;  $n = 19$  (CON<sub>15m</sub>), 14 (CR<sub>15m</sub>), 6 (CON<sub>20m</sub>), and 8 (CR<sub>20m</sub>) mice. **(F)** Kaplan–Meier  
1056 plot for the inverted grid-hang test performed prior to endpoint measures at 30 months of age  
1057 for the middle-aged group;  $n = 11$  (10mCON), 18 (CON<sub>15m</sub>), and 13 (CR<sub>15m</sub>) mice. **(G)** Twenty-  
1058 four hours of voluntary running-wheel distance;  $n = 16$  (CON<sub>15m</sub>), 13 (CR<sub>15m</sub>), 6 (CON<sub>20m</sub>), and  
1059 9 (CR<sub>20m</sub>) mice. Glucose tolerance test parameters including **(H)** blood glucose response to 2  
1060  $\text{mg}\cdot\text{kg}^{-1}$  glucose injection (I.P.), **(I)** peak glucose and **(J)** area under the curve/glucose tolerance.  
1061 **(K)** Whole-body metabolic analysis of energy expenditure normalized to body surface area  
1062 (upper), mean X-Y-Z activity (middle) and respiratory exchange ratio ( $\text{VCO}_2/\text{VO}_2$ ; lower)  
1063 reported every 2 h across one full day (white)/night (black) cycle in the month prior to endpoint  
1064 measures;  $n = 12$  (10mCON), 9 (30mCON), and 7 (30mCR) mice. Data are presented as  
1065 mean  $\pm$  SEM. Two-way repeated-measure ANOVA with Tukey post hoc tests (B–E, G–H, K),  
1066 Mantel–Cox log rank (F), and one-way ANOVA with Fisher’s LSD post hoc tests (I–J) was  
1067 used to compare the data. \*, \*\*, and \*\*\* denote a significant difference between groups  
1068 of  $P < 0.05$ ,  $P < 0.01$ , and  $P < 0.001$ , respectively. Colored asterisks refer to the group of  
1069 comparison.

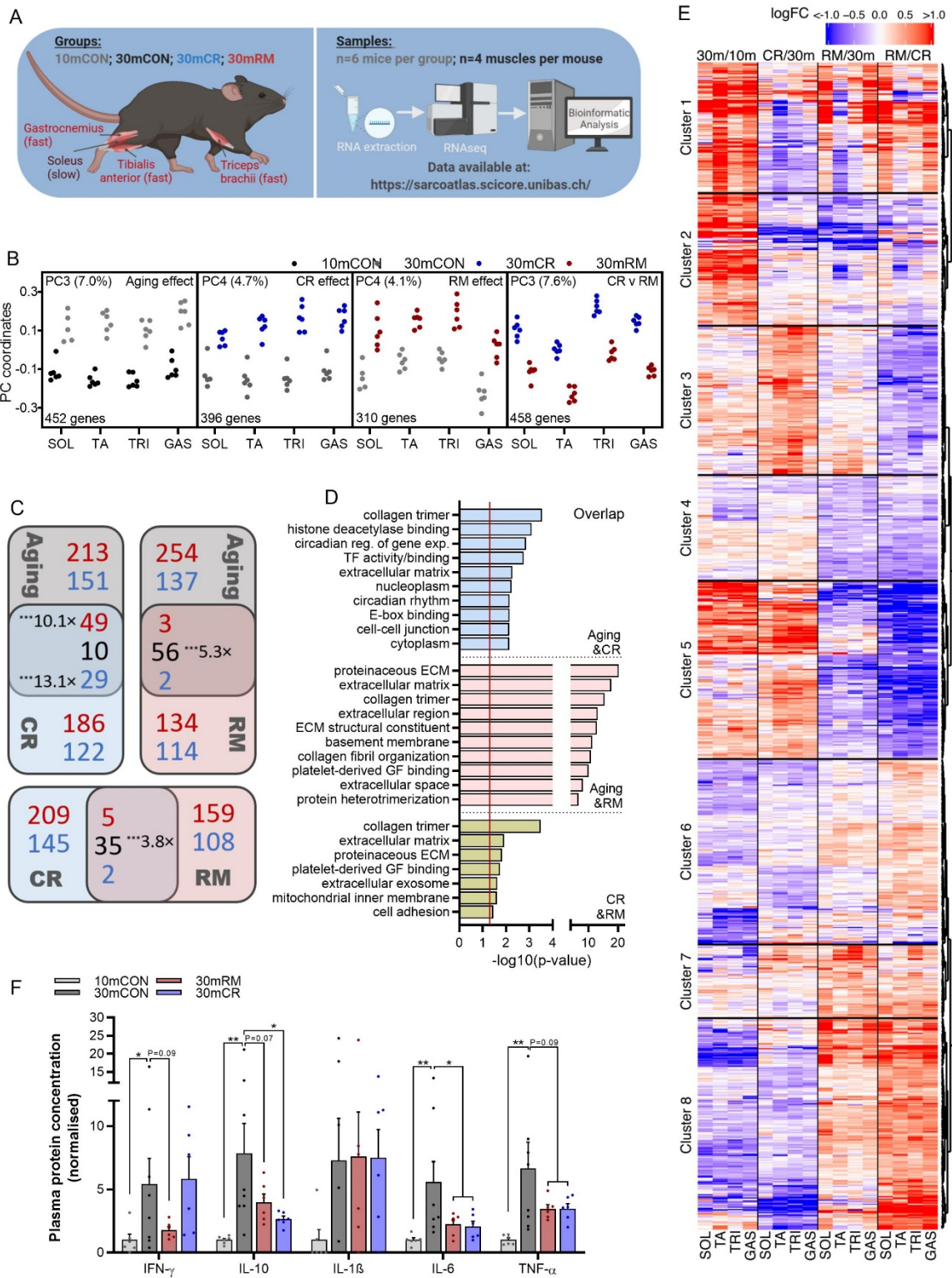
1070

1071 **Figure 2**



1073 **Figure 2: CR promotes a fast-to-slow muscle fiber phenotype shift. (A)** Muscle mass for  
1074 *quadriceps* (QUAD), *gastrocnemius* (GAS), *tibialis anterior* (TA), *plantaris* (PLA), *extensor*  
1075 *digitorum longus* (EDL), *soleus* (SOL), and *triceps brachii* (TRI) was averaged across both  
1076 limbs, normalized to body mass and then to 10-month-old control mice. **(B)** Scatterplots and  
1077 linear regressions of the relationship between body and muscle mass of the fast twitch TA, TRI,  
1078 GAS, QUAD and EDL muscles and the slow twitch SOL muscle. Isolated muscle function  
1079 parameters, including **(C)** force-frequency curve (left) and fatigue response to multiple  
1080 stimulations (right), **(D)** peak force normalized to body mass, **(E)** peak force normalized to  
1081 cross sectional area (specific force), and **(F)** mean twitch responses including time-to-peak  
1082 tension (TPT), half-relaxation time (1/2-RT) and peak twitch (Pt) for SOL (top panel) and EDL  
1083 muscle (bottom panel). **(G)** Proportional total fiber-type-specific cross-sectional area analyzed  
1084 on whole cross sections of (left to right) SOL (n=6), EDL (n=7, 9 and 8), TA (n=11, 13 and 7)  
1085 and TRI (n=5, 9 and 9) for 10mCON, 30mCON and 30mCR, stained with antibodies against  
1086 type I (blue), type IIA (yellow), and type IIB (green) fibers as well as laminin (red), while fibers  
1087 without staining were classified as IIX. **(H)** Representative images for SOL, EDL, TA and TRI.  
1088 Group numbers for 10mCON are  $n = 17$  (a, b), 10 (c-f: EDL) and 8 for fatigue, 11 (c-e: SOL)  
1089 or 9 for fatigue, for 30mCON  $n = 20$  (a, b), 19 (c-f: EDL), 15 (c-e: SOL) and 16 (f: SOL), and  
1090 for 30mCR  $n = 20$  (a, b), 18 (c-e: EDL), 15 (c-e: SOL) or 13 for fatigue, 12 (f: SOL) and 15 (f:  
1091 EDL). Data are presented as mean  $\pm$  SEM. One-way (a and d-f) or two-way repeated- measure  
1092 (c, g) ANOVAs with Fisher's LSD or Tukey's post hoc tests, respectively, were used to  
1093 compare between data. \*, \*\*, and \*\*\* denote a significant difference between groups  
1094 of  $P < 0.05$ ,  $P < 0.01$ , and  $P < 0.001$ , respectively. Colored asterisks refer to the group of  
1095 comparison.

1096 **Figure 3**

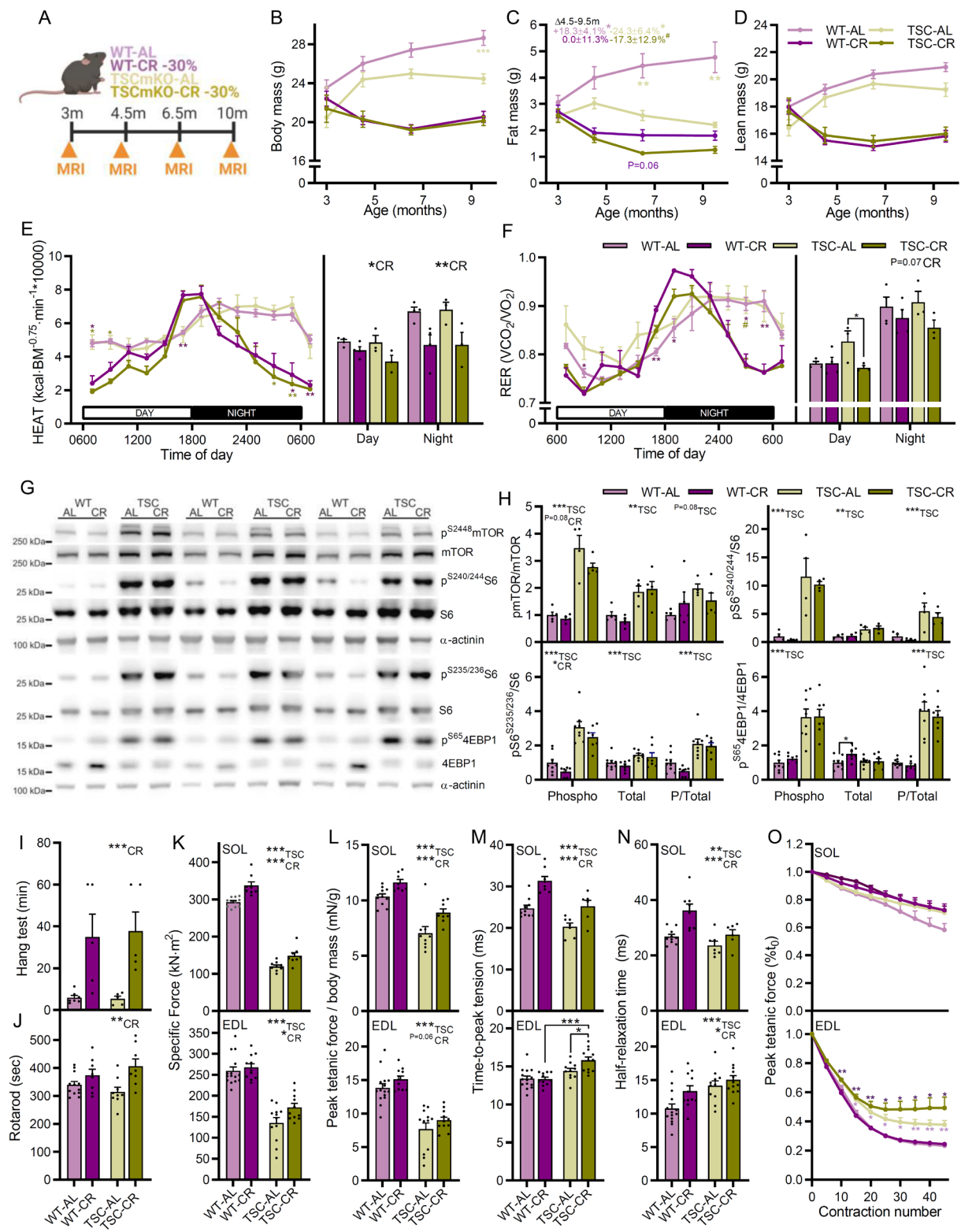




1098 **Figure 3: CR and RM induce distinct gene expression signatures.** (A) Scheme of treatment  
1099 groups, muscles, and numbers of samples used in sequencing analysis. Data for 10mCON,  
1100 30mCON, and 30mRM have been previously reported (Ham & Börsch et al. 2020). (B)  
1101 Coordinates of principal components representing aging (PC3 for 10mCON and 30mCON) CR  
1102 (PC4 for 30mCON and 30mCR), RM (PC4 for 30mCON and 30mRM) and CR vs. RM (PC3  
1103 for 30mCR and 30mRM) effects for gene expression collected in *soleus* (SOL), *tibialis*  
1104 *anterior* (TA), *triceps brachii* (TRI) and *gastrocnemius* (GAS). The numbers associated with  
1105 the PCs indicate the fraction of the variance in gene expression in samples along the  
1106 corresponding PC. Each dot corresponds to one muscle sample, from an individual animal. The  
1107 number of genes aligned with each PC is displayed in the bottom left corner of each graph. A  
1108 gene was considered aligned with a PC if the absolute value of the Pearson correlation  
1109 coefficient between the expression of the gene and PC coordinates was  $\geq 0.4$ , and the absolute  
1110 value of the  $z$  score of the projection of the gene expression on a PC was  $\geq 1.96$ . (C) Pairwise  
1111 Venn diagram comparisons of genes significantly aligned to aging, CR and RM effects.  
1112 Numbers in red, blue and black represent increasing, decreasing and oppositely regulated genes,  
1113 respectively. Where the overlap of genes is significantly above that expected by chance, the  
1114 level of significance and representation factor are noted. (D) Top-ten DAVID gene ontology  
1115 terms enriched ( $P < 0.05$ ) for genes aligned to both aging and CR effects, aging and RM effects  
1116 or CR and RM effects. Enrichment significance threshold was set at  $P < 0.05$  (gray and red  
1117 dashed lines). (E) Heatmap of fold-changes for genes aligned with any of the four PCs described  
1118 in (B) for aging (30mCON/10mCON), CR (30mCR/30mCON), RM (30mRM/30mCON) and  
1119 CR vs. RM (30mRM/30mCR) effects in all four muscles. Hierarchical clustering based on the  
1120 Euclidean distance of these changes rendered 8 gene clusters. (F) Plasma cytokine protein  
1121 concentration. Data are displayed as fold-change from 10mCON group. Cytokine levels  
1122 between the detection limit were set as 0. For the sarcopenia data set,  $n = 6$  mice per muscle per  
1123 group, except for SOL 30mCON where one data point was removed due to a technical error. A  
1124 modified Fisher's exact test was used to determine significance.

1125

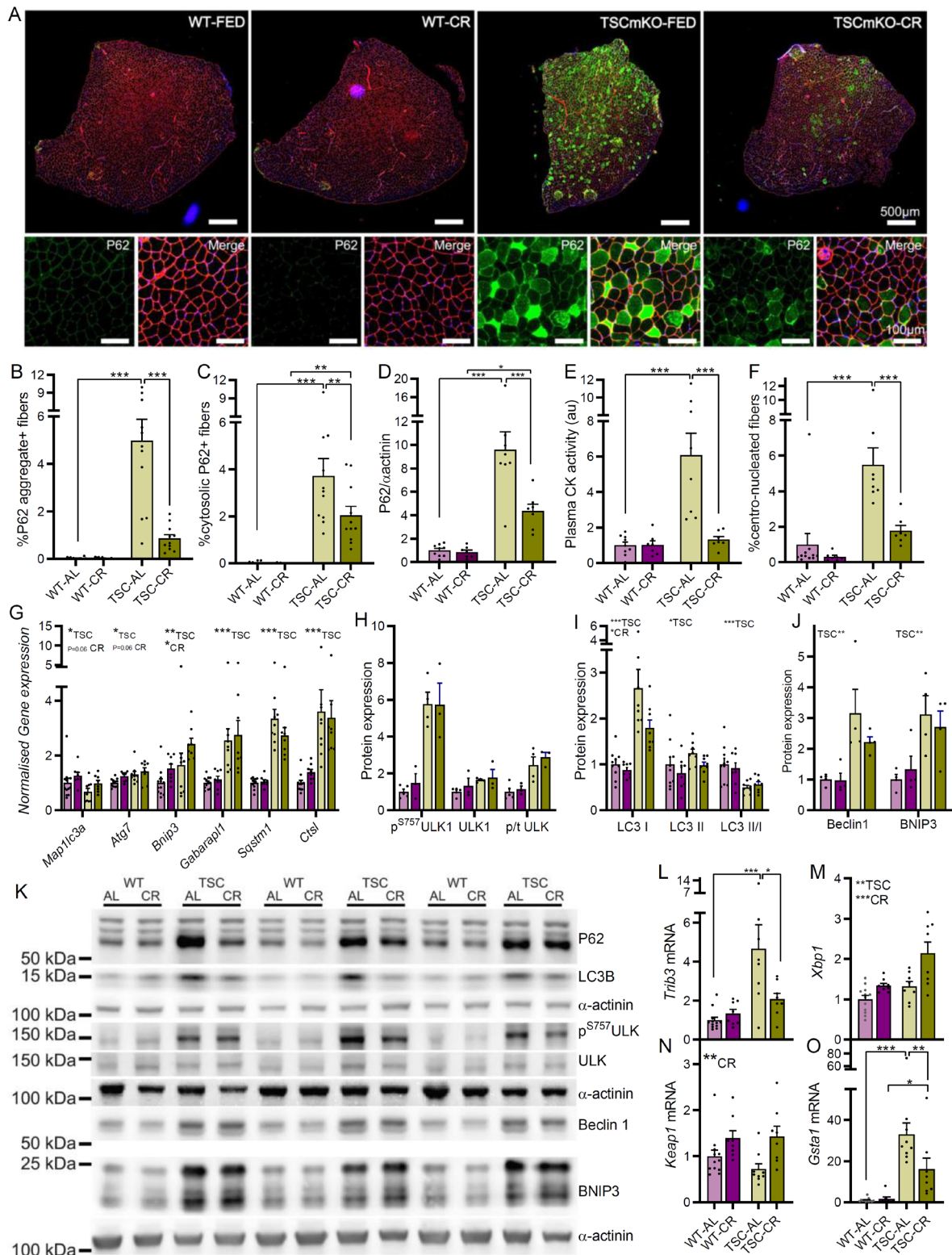
1126 **Figure 4**



1128 **Figure 4: CR improves muscle function without suppressing mTORC1 activity in the**  
1129 **TSCmKO model of accelerated muscle aging. (A)** Experimental design schematic showing  
1130 experimental groups as well as time course of physiological measures. **(B)** Body mass **(C)**  
1131 whole-body fat mass and **(D)** lean mass for WT and TSCmKO mice fed *ad libitum* (WT-AL  
1132 and TSC-AL) or 70% of *ad libitum* (WT-CR and TSC-CR) beginning at 3 months of age. **(E)**  
1133 Whole-body metabolic analysis of energy expenditure normalized to body surface area and **(F)**  
1134 respiratory exchange ratio ( $VCO_2/VO_2$ ; lower) reported every 2 h across one full day  
1135 (white)/night (black) cycle (left) and day and night-time averages (right) in the month prior to  
1136 endpoint measures;  $n = 12$  (10mCON), 9 (30mCON), and 10 (30mCR) mice. **(G)** Representative western blot analysis of mTORC1 pathway components in WT-AL, WT-  
1138 CR, TSC-AL and TSC-CR *gastrocnemius* (GAS) muscle. Similar results were obtained for  
1139 each protein across three separate gels with different samples. **(H)** Quantification of western  
1140 blots showing the abundance of phosphorylated protein normalized to total protein for mTOR  
1141 (upper left) S6 (upper right and lower left) and 4EBP1 (lower right). **(I)** Inverted grid hang time  
1142 and **(J)** time spent on a rotating rod. Isolated muscle function parameters for SOL (upper panel)  
1143 and EDL (lower panel), including **(K)** specific force, **(L)** peak tetanic force normalized to body  
1144 mass, **(M)** twitch time-to-peak tension and **(N)** half-relaxation time as well as **(O)** fatigue  
1145 response to multiple stimulations. Data are presented as mean  $\pm$  SEM. Two-way ANOVAs with  
1146 Tukey post hoc tests were used to compare the data. \*, \*\*, and \*\*\* denote a significant  
1147 difference between groups of  $P < 0.05$ ,  $P < 0.01$ , and  $P < 0.001$ , respectively. # denotes a trend  
1148 where  $0.05 < P < 0.10$ . Colored asterisks refer to the group of comparison.

1149

1150 **Figure 5**



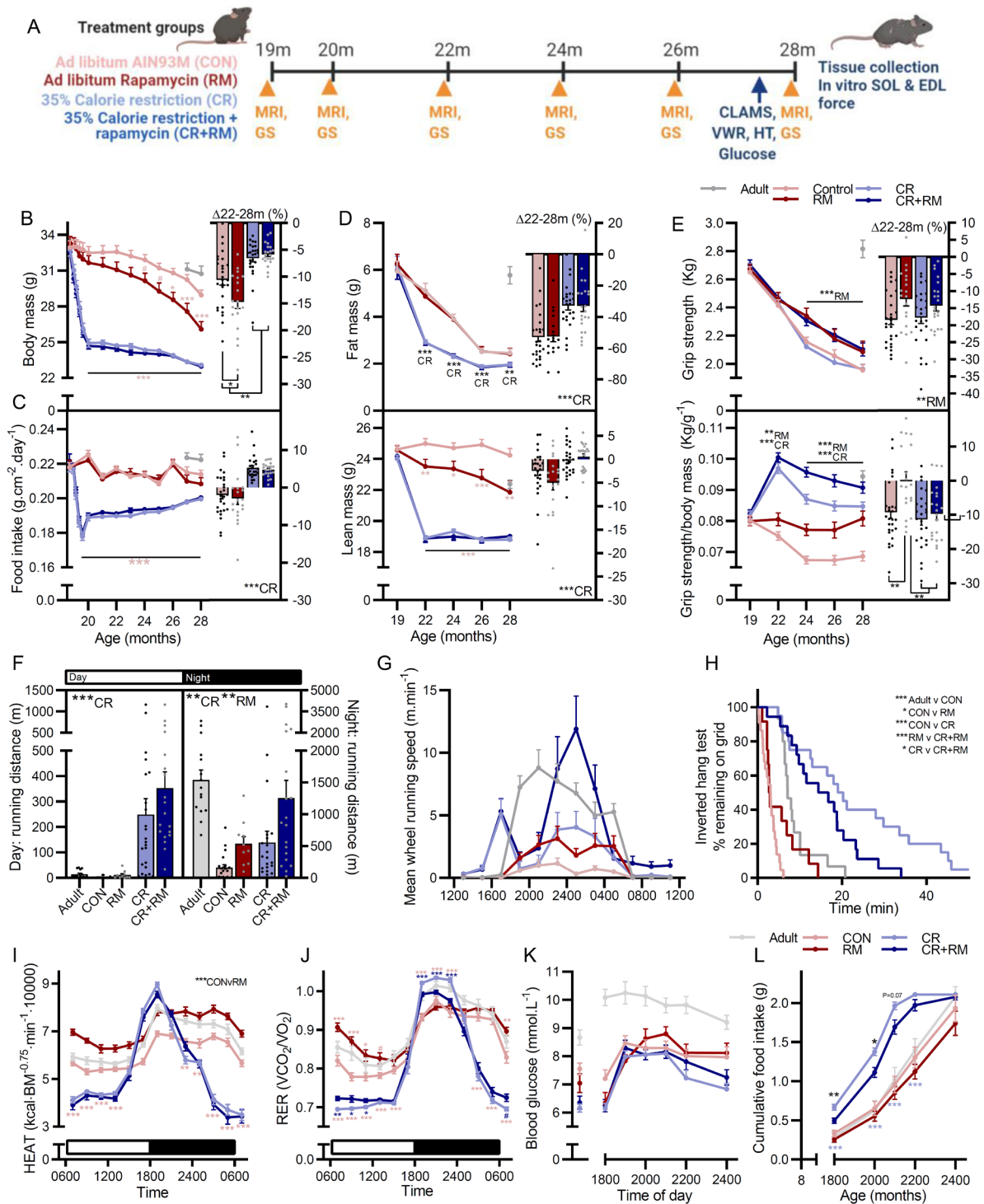
1151

1152

1153 **Figure 5: CR attenuates P62 accumulation and improves muscle integrity in TSCmKO**  
1154 **mice. (A)** Representative tibialis anterior (TA) cross sections stained with antibodies against  
1155 P62 and laminin and counterstained with DAPI. Quantification of fibers with **(B)** P62+  
1156 aggregates and **(C)** P62+ cytosolic staining. **(D)** Western blot quantification of P62 protein  
1157 expression in gastrocnemius muscle. **(E)** Plasma creatine kinase activity and **(F)** percentage  
1158 centro-nucleated fibers in WT-AL, WT-CR, TSC-AL and TSC-CR mice. **(G)** RT-qPCR  
1159 analysis of autophagy associated genes in gastrocnemius muscle. Western blot quantification  
1160 of the abundance of **(H)** phosphorylated and total ULK1 protein, **(I)** LC3I, LC3II and the ratio  
1161 of LC3II to I and **(J)** beclin1 and BNIP3 protein as well as **(K)** representative gels. RT-qPCR  
1162 analysis of ER-stress and autophagy interacting genes including **(L)** Trib3, **(M)** Xbp1, **(N)**  
1163 Keap1 and **(O)** Gsta1. Data are presented as mean  $\pm$  SEM. Two-way ANOVAs with Tukey post  
1164 hoc tests were used to compare data. \*, \*\*, and \*\*\* denote a significant difference between  
1165 groups of  $P < 0.05$ ,  $P < 0.01$ , and  $P < 0.001$ , respectively. # denotes a trend where  
1166  $0.05 < P < 0.10$ . Colored asterisks refer to the group of comparison.

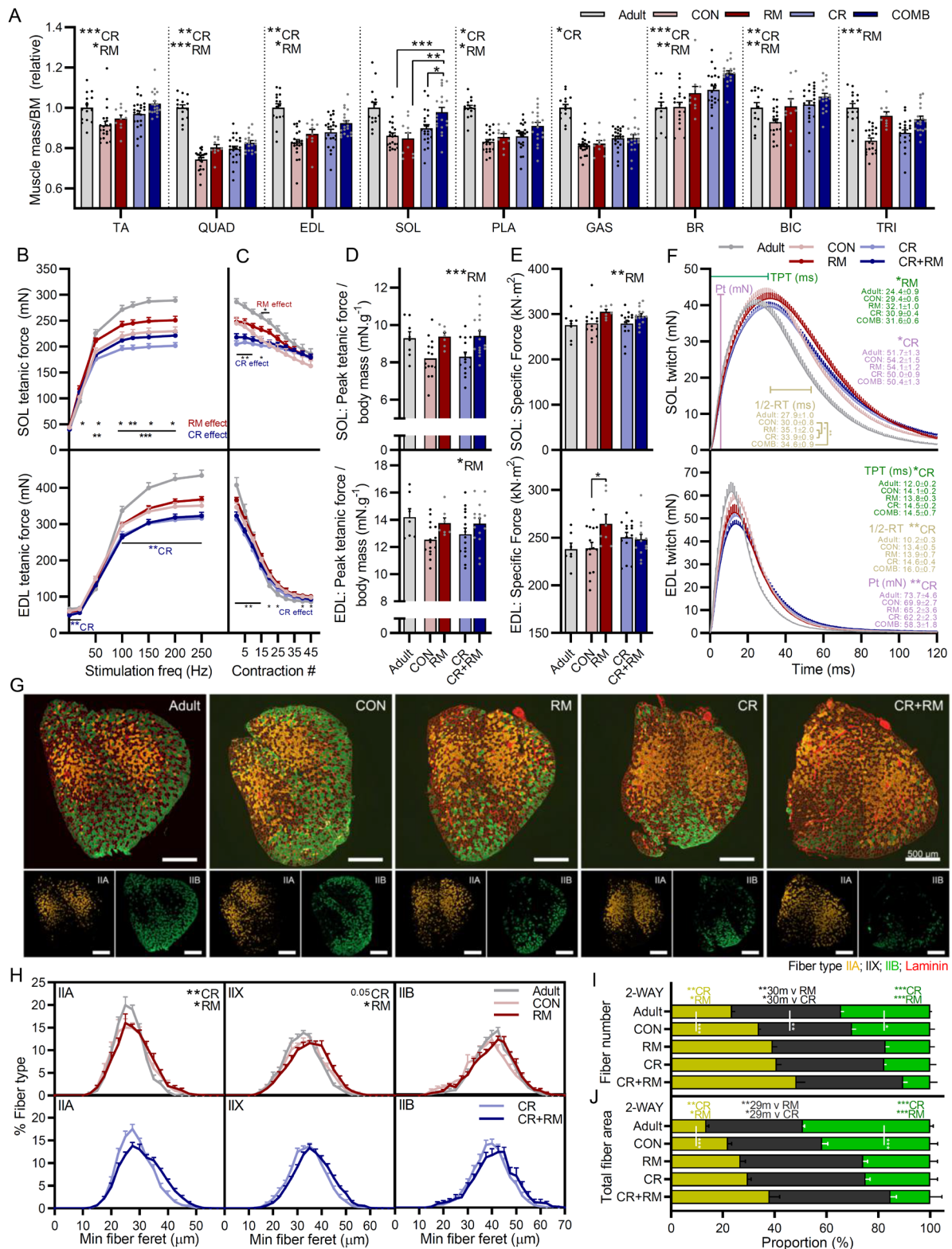
1167

1168 **Figure 6**



1170 **Figure 6. RM and CR exert distinct and additive effects on whole-body muscle function**  
1171 **and metabolism. (A)** Experimental design schematic showing experimental groups as well as  
1172 time course of physiological measures. Repeated measures (left) of **(B)** body mass, **(C)**  
1173 intake normalized to body surface area, **(D)** whole-body fat (upper) and lean (lower) mass as  
1174 well as **(E)** absolute (upper) and body mass normalized (lower) all-limb grip strength measured  
1175 across the treatment period from 19 to 28 months as well as the percentage change between 22  
1176 months after adaptation to CR and 28 months (right). **(F)** Day and night-time voluntary running  
1177 distance and **(G)** running speed patterns across a 24 hour period, as well as **(H)** Kaplan–Meier  
1178 plot for the inverted grip-hang test performed prior to endpoint measures at 28 months. Whole-  
1179 body metabolic analysis of **(I)** energy expenditure normalized to body surface area and **(J)**  
1180 respiratory exchange ratio reported every 2 h across one full day (white)/night (black) cycle in  
1181 the month prior to endpoint measures. **(K)** blood glucose levels and **(L)** voluntary food intake  
1182 over the night-time feeding period following a day-time fast in 10mCON, 28mCON, 28mRM,  
1183 28mCR and 28mCR+RM groups. Data are presented as mean  $\pm$  SEM. Two-way ANOVAs with  
1184 Tukey post hoc tests (A–G and I–L) and Mantel–Cox log rank tests (H) were used to compare  
1185 the data. \*, \*\*, and \*\*\* denote a significant difference between groups of  $P < 0.05$ ,  $P < 0.01$ ,  
1186 and  $P < 0.001$ , respectively. # denotes a trend where  $0.05 < P < 0.10$ . Colored asterisks refer to  
1187 the group of comparison.

1188 **Figure 7**





1190 **Figure 7. CR and RM have additive effects on muscle mass, function and fiber size and**  
1191 **composition. (A)** Muscle mass for tibialis anterior (TA), *quadriceps* (QUAD), *extensor*  
1192 *digitorum longus* (EDL), *soleus* (SOL), *plantaris* (PLA), *gastrocnemius* (GAS), brachioradialis  
1193 (BR), biceps brachii (BIC) and *triceps brachii* (TRI) were averaged across both limbs,  
1194 normalized to body mass and then to 10-month-old control mice. Isolated muscle function  
1195 parameters, including **(B)** force-frequency curve and **(C)** fatigue response to multiple  
1196 stimulations, **(D)** peak force normalized to body mass, **(E)** peak force normalized to cross  
1197 sectional area (specific force), and **(F)** mean twitch responses including time-to-peak tension  
1198 (TPT), half-relaxation time (1/2-RT) and peak twitch (Pt) for SOL (top panel) and EDL muscle  
1199 (bottom panel). **(G)** Representative cross sectional images along with **(H)** fiber-type specific  
1200 minimum fiber feret distribution showing *ad libitum*-fed (upper) and calorie restricted (lower)  
1201 groups, **(I)** fiber type-specific fiber numbers and **(J)** total fiber type-specific cross sectional area  
1202 of the forelimb muscle brachioradialis (BR) stained with antibodies against type I (blue), type  
1203 IIA (yellow), and type IIB (green) fibers as well as laminin (red), while fibers without staining  
1204 were classified as IIX. Data are presented as mean  $\pm$  SEM. Two-way repeated- measure  
1205 ANOVAs with Tukey's post hoc tests were used to compare between data. \*, \*\*, and \*\*\* denote  
1206 a significant difference between groups of  $P < 0.05$ ,  $P < 0.01$ , and  $P < 0.001$ , respectively.  
1207 Colored asterisks refer to the group of comparison.